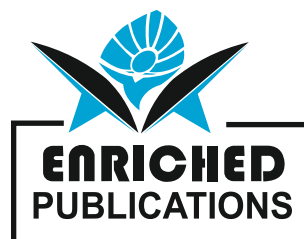


Journal of Mechanics and Thermodynamics

**Volume No. 11
Issue No. 1
January - April 2023**



ENRICHED PUBLICATIONS PVT. LTD

**S-9, IInd FLOOR, MLU POCKET,
MANISH ABHINAV PLAZA-II, ABOVE FEDERAL BANK,
PLOT NO-5, SECTOR-5, DWARKA, NEW DELHI, INDIA-110075,
PHONE: - + (91)-(11)-47026006**

Journal of Mechanics and Thermodynamics

Aims and Scope

Journal of Mechanics and Thermodynamics publishes theoretical and practice oriented papers, dealing with problems of modern technology (power and process engineering, structural and machine design, production engineering mechanism and materials, etc.), Materials and Design Engineering, Vibration and Control, Thermal Engineering and Fluids Engineering.

Journal of Mechanics and Thermodynamics

**Managing Editor
Mr. Amit Prasad**

Editor in Chief

Dr. Syed Fahad Anwer
IIT, Kanpur
sfahadanwer@zhcet.ac.in

Journal of Mechanics and Thermodynamics

(Volume No. 11, Issue No. 1, January - April 2023)

Contents

Sr. No	Article/ Authors	Pg No
01	Study of Cyclic High Temperature Oxidation Behaviour of Bare and Ni-Cr Coating Over Low Alloy Steel <i>- Jitendra Kumar Pal, Shivam Trivedi</i>	1 - 8
02	Simulation of MHO Characteristics for Transmission Line Protection using PSCAD <i>- Yashasvi B, Vidushi K, Ramesh P</i>	9 - 18
03	Design of Morphological Approach to Detect and Eliminate Ink Bleed in Document Images <i>- Kusum Grewal , Renu Malhan</i>	19 - 26
04	Thermal-hydraulic Analysis of Fuel Rod of A TRIGA Mark II Research Reactor <i>- Md. Shafiqul Islam, Abid Hossain Khan</i>	27 - 46
05	Empirical Models for Predicting Global Solar Radiation using Meteorological Parameters for Sokoto, Nigeria <i>- Davidson O. Akpootu, Bello I. Tijjani, Usman M. Gana</i>	47 - 69

Study of Cyclic High Temperature Oxidation Behaviour of Bare and Ni-Cr Coating over Low Alloy Steel

Jitendra Kumar Pal¹, Shivam Trivedi^{1*}

Mechanical Engineering Department, Faculty of Engineering and Technology, Rama University, Kanpur, Uttar Pradesh, India

Assistant Professor, Mechanical Engineering Department, FET, Rama University, Kanpur, Uttar Pradesh, India

ABSTRACT

Oxidation behaviour of low carbon and low alloyed steels at different Ni-Cr coatings thickness are studied, and also resistance offered by different coating thickness is also investigated. Hardness of low alloy steel was found to be increased from 202 to 342 VHN after the application of coatings. Parabolic rate constant (K_p) for high temperature oxidation of bare, 200-250 μ m, and 250-300 μ m thick Ni-Cr coated low alloy steel were calculated to be 787.192, 0.235608, and 0.501787 ($\times 10^{-10} \text{g}^2 \text{cm}^{-4} \text{s}^{-1}$) respectively.

Keywords: Oxidation; high temperature; thermal spray coatings; D-gun spray.

1. INTRODUCTION

Oxidation is the reaction between metal and air or oxygen in dry medium. Virtually every metals and alloys react with air, and rate of oxidation increases with increase in temperature [1]. Thus, in engineering applications oxidation resistance at elevated temperature must be taken into consideration in gas turbine, rocket engines, furnaces, petro-chemical systems etc. It is difficult to evaluate economical losses caused due to oxidation. Some of them are plant downtime, loss of product, loss of efficiency, contamination, overdesign etc. These issues can be resolved by taking number of preventive measures such as controlling process parameters, fuel selection, design aspects, chemical additive, use of inhibitors etc. One of the economical, efficient and reliable ways to control the oxidation problem is the application of a thin layer coating of oxidation resistant material over the components exposed to oxidising environment. Coatings with good thermal conductivity may enhance the service life of the components without affecting the thermal efficiency of the system. Thermal spraying coating technique can provide protection to the underlying substrate by producing a protective oxide layer at elevated temperatures. Detonation-gun (D-gun) technique is one of the efficient thermal spraying techniques that provide hard, wear resistant and dense micro-structured coatings and is considered as best thermal spraying technique in terms of coating density and porosity. Hence, D-gun spray coating is used to deposit coatings on heat facing components of the large units. Coating enhances the life-time of the material up to 10 times of coatings cost. The composition and structure of the coatings depend on exposed environments [2]. Ni-Cr coatings have high temperature oxidation resistance properties in oxidising environment [3]. During the service life of components, applied coatings are expected to form slow growing protective oxides on the exposed surface. These protective oxides should not allow the

corrosive species to diffuse into the coating and to reach the substrate material, which results in the failure of the system [4]. Cyclic oxidation of Ti3Al-based alloy (Ti–24Al–11Nb) with a thin 80Ni–20Cr (at.%) protective coating were carried out at 600°C and 900°C in air. Ni-Cr layer formed protective oxide scale and prevented Ti diffusion into substrate material, resulted improved oxidation resistance. Cr has higher affinity to oxygen as compared to Ni and formed more stable Cr₂O₃. Also, oxidation rate was found to be faster at 900°C as compared to that of at 600°C [5].

Oxidation behaviour of bare and cold sprayed Ni-Cr coated (Ni-20Cr, Ni-50Cr) SAE 213-T22 boiler steel were studied at 900°C and observed intense spalling and peeling off its oxide scale in bare specimen, due to the formation of un- protective (Fe₂O₃) oxide scale. Coated steel showed better oxidation resistance as compared to the uncoated steel. Author also observed that Ni-50Cr coated steel showed better oxidation resistance as compared to Ni-20Cr coated steel. This oxidation resistance was due to the formation of spinels and oxides of nickel and chromium [6].

Rajput et al. studied the hot deformation behaviour of low carbon and low alloyed steel and determine the safe workability region [7-9]. There are scarce of literature that reported the cyclic high temperature oxidation behaviour of D-gun sprayed Ni-Cr coated low carbon and low alloyed steels (boiler and tube materials). Also the study of resistance offered by different coating thicknesses (200-250 µm and 250-300 µm) of D-gun sprayed Ni-Cr coating were lacking. Hence, there is need to investigate the oxidation behaviour of low carbon and low alloyed steels in a comprehensive manner. In this work, oxidation behaviour of low carbon and low alloyed steels at different Ni-Cr coatings thickness are studied at 750°C, and also investigate the resistance offered by different coating thickness.

2. EXPERIMENTAL PROCEDURE

Low alloyed was procured in the form of rectangular sheet. Chemical compositions of substrate materials was determined using Spark spectroscopy and represented in Table 1, respectively.

Table 1. Chemical composition of low alloy steel.

ELEMENTS	C	Mn	Si	Ti	P	Ni	Cr	Al	Fe
Wt. %	0.084	1.12	0.211	0.014	0.023	0.031	0.038	0.037	Bal.

Specimens were cut in the dimensions of 15 x 15 x 5mm, followed by polishing using 320, 600, 1000, 1200 and 1500 grit size polishing papers. Before application of coatings, the specimens were degreased with the help of acetone. D- gun spray technique was used to deposit the Ni-Cr coating over the specimens. Coatings were deposited on the specimens in the thickness ranging of 200-250 µm and 250-300 µm on the six faces of the low alloy specimens at SVX Powder M Surface Pvt. Ltd., Greater Noida. Mechanical interlocking is the main mechanism of thermal spray coating adhesion/adherence.

High temperature oxidation study of bare and Ni-Cr coated low alloy specimens were conducted in a laboratory muffle furnace at a temperature of $750\pm 10^\circ\text{C}$ for 50 cycles with holding time 1 h. Specimens were kept in alumina boats during the experiments. The boats used for the study were preheated at a constant temperature of 1000°C for 10 h, with the assumption that the weight of the boat would remain constant during the course of high temperature study. Specimens were weighing after each cycle with the help of electronics weighing machine (DAB 220). Hardness were performed on bare and Ni-Cr coated specimens at 5 kg load and with dwell time 10 s with the help of Vickers hardness testing machine (VM-50). Scanning electron microscope (Carl Zeiss EVO 50) was used to study images, EDS and elemental mapping of the specimens.

3. RESULTS AND DISCUSSION

3.1. Low alloyed steel

Splat-like layered morphologies was present in the coatings due to the deposition and re-solidification of molten or semi molten powder particles. There were no indications of micro cracks in the microstructures. The dark spots in the coating/coating substrate interface were mostly inclusions (Fig. 1). The circular jet-black dark dots were expected to be porosity. Some micro-pores were present and randomly distributed in the coatings. Further all the coatings irrespective of coating powder composition were found to be free from any visible surface cracks. The coatings in general had smooth surfaces. Energy dispersive x-ray spectroscopy (EDS) and elemental mapping of as-sprayed 250- 300 μm thick Ni-Cr coated low alloy steel specimen is shown in the fig. 1. Value of average hardness of bare low alloyed steel specimen was 202 VHN. Hardness increased rapidly with application of coatings from 202 VHN to 342 VHN.

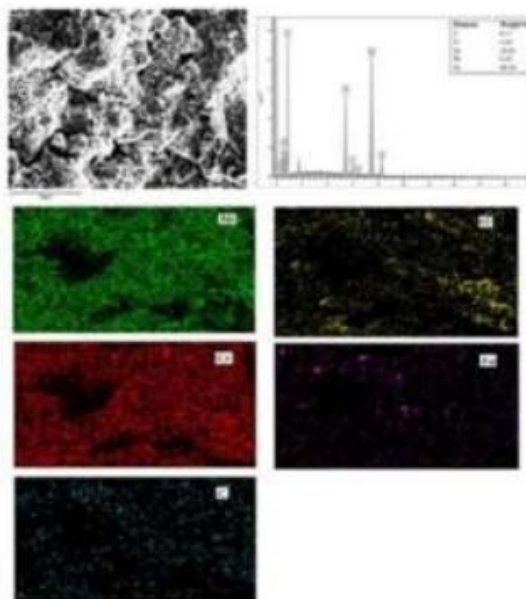


Figure 1. EDS (area analysis) and elemental mapping of as sprayed 250-300 μm thick NiCr coating on low alloy steel.

Ni-Cr coated specimens showed minor weight gain up to 50th cycle, whereas high weight gains were observed in case of bare low alloy steel starting from 1st cycle and continued till 50th cycle. During oxidation of bare low alloy steel, scale formation was noticed at the end of 1st cycle and swelling of the scale was observed at the end of 13th cycle. Oxidized bare low alloy steel had irregular scales with cracks at the edges. The fragile scale formed over the surface of the bare steel that could not sustained, and started peeling off from the surface. Minor spalling of scale started at the end of 27th cycle for bare specimens. However, the scale formation continued till 50th cycle. Also some metallic sound was observed during cooling. Coated low alloy steel showed a continuous and defect free interfacial contact with the substrate steel. The colour of oxide formed just after 1st cycle over the bare and coated low alloy steel specimens was dark gray which remained till the completion of 50th cycle.

Fig. 2 shows the surface morphology (EDS and elemental mapping) of the bare and D-gun sprayed Ni-Cr coated low alloy steel specimens of different coating thickness after 50 cycles at 750±10°C. Elemental mapping analysis of oxidized bare specimen shows scale rich in Fe and O as shown in fig. 2(a). This indicates the formation of iron oxides (Fe/FeO/Fe₃O₄/Fe₂O₃). Small content of Fe was observed at the top layer of the coated specimen probably due to diffusion as shown in fig. 2(b) and 2(c). Scale formed over the bare specimen after 50 cycles was amorphous in appearance, and composed of peeled off particles. EDS results of coated specimens reported large amount of Cr and O and marginal amount of Ni at the points of analysis. This represents that the exposed areas of the scale seemed to be adherent in the case of coated specimens. Thus, the coated specimens were good oxidation resistance as no scaling was observed till the completion of 50th cycle, while the bare specimens were totally consumed.

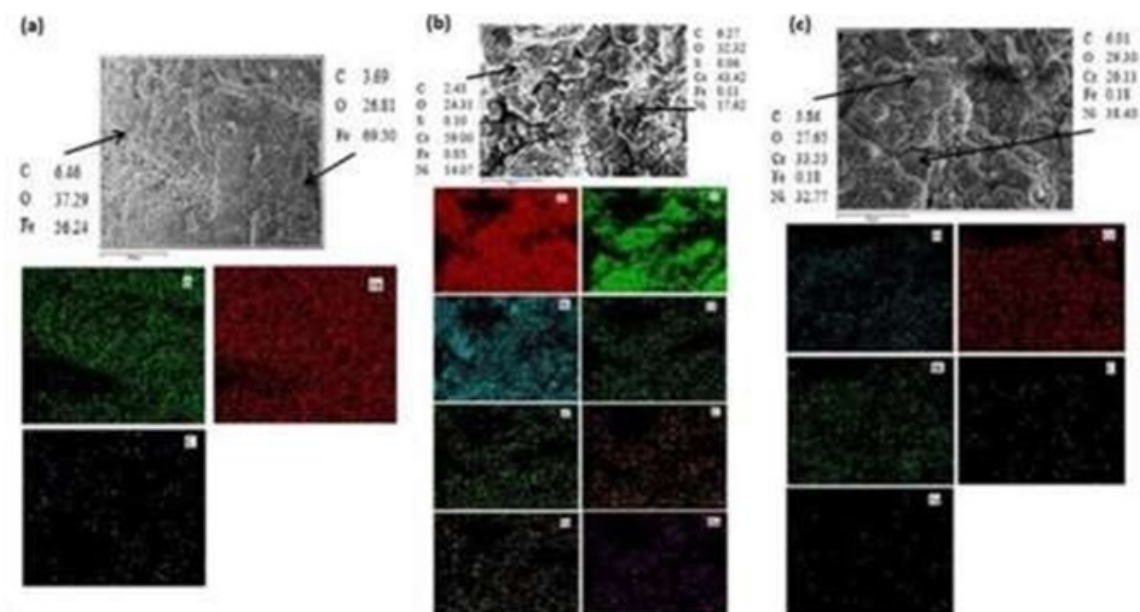


Figure 2.EDS spectrum and elemental mapping of (a) bare, (b) 200-250 μm, and (c) 250-300 μm, thick NiCr coated low alloy steel after high temperature oxidation of 50 cycles.

3.1.1. Evaluation of oxidation rate

Fig. 3 shows the graph between cumulative weight gains per unit surface area (mg/cm²) vs. number of cycles for the low alloy steel specimens subjected to high temperature oxidation at 750±10°C. Graph indicates that Ni-Cr coated low alloy steel specimens attained marginal weight gain till 50th cycle, whereas high weight gain was observed bare low alloy steel specimen. Overall weight gain after 50 cycles of high temperature oxidation for the bare, 200-250 µm, and 250-300 µm thick Ni-Cr coated low alloy steel specimens were calculated to be 118.44759, 2.1428, and 3.24849 mg/cm², respectively. Overall weight gain in 250-300 µm thick Ni-Cr coated was higher as compared to 200-250 µm thick Ni-Cr coated specimens because bond strength decreased with increase in coating thickness results corrosive media penetrates easily in higher thickness. Therefore 200-250 µm thick Ni-Cr coated specimens showed better resistance against high temperature oxidation in comparison to 250-300 µm thick Ni-Cr coated low alloy steel. Further, square of weight gain (mg²/cm⁴) vs. number of cycles graph was plotted for the low alloy steel specimens as shown in fig. 4. Parabolic rate constant (K_p) values were calculated by fitting the plotted curves with the linear regression.

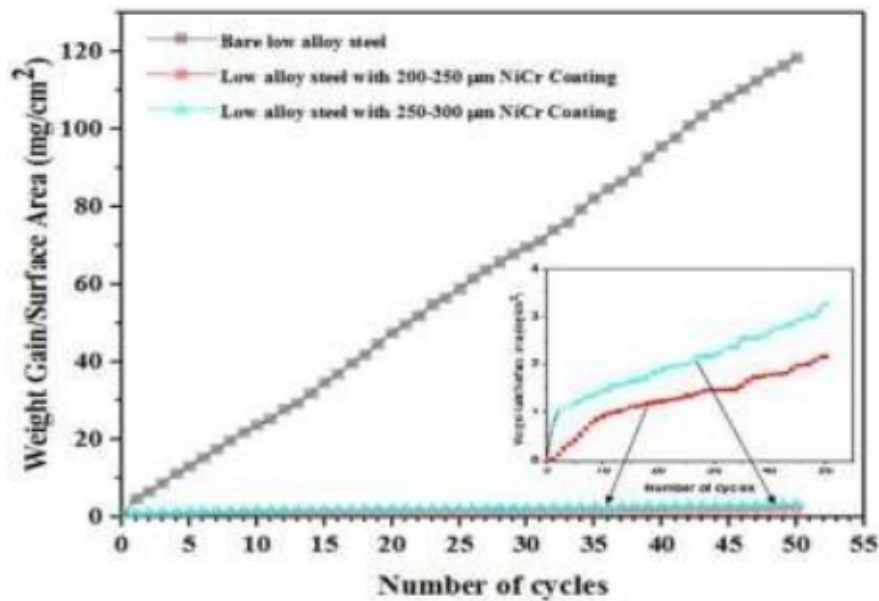


Figure 3. Weight change/surface area (mg/cm²) vs number of cycles graph of low alloy steel subjected to high temperature oxidation after 50 cycles.

In 1993, Wanger showed that ideal ionic diffusion-controlled oxidation of pure metals should follow a parabolic oxidation rate law as represented by equation (1) [6].

$$W^2 = k_p t + C \quad (1)$$

where W is the weight gain per unit area, t is time, k_p is the parabolic rate constant, and C is a constant.

Metals demonstrating a parabolic oxidation rate yield a straight line when the data are plotted as W^2 versus time. It can be concluded from fig. 4 that Ni-Cr coated specimens follow nearly a parabolic rate law. The parabolic rate constants (K_p) for bare, 200-250 μm , and 250-300 μm thick Ni-Cr coated low alloy steel specimens are shown in Table 3. Parabolic rate constant of coatings was found to be very small in comparison to that of bare steel specimen, indicating the protective nature of the coatings against high temperature oxidation. Since, lower the value of K_p , better the oxidation resistance.

Table 3. Parabolic rate constant (K_p) of oxidized low alloy steel.

Specimen	K_p ($10^{-10} \text{ g}^2/\text{cm}^4/\text{s}$)
Bare low alloy steel	787.192
200-250 μm thick Ni-Cr coated low alloy steel specimens	0.235608
250-300 μm thick Ni-Cr coated low alloy steel specimens	0.501787

The correlation coefficients for bare, 200-250 μm , and 250-300 μm thick Ni-Cr coated low alloy steel specimens were 0.96, 0.98, and 0.98 respectively, as shown in the fig. 4.

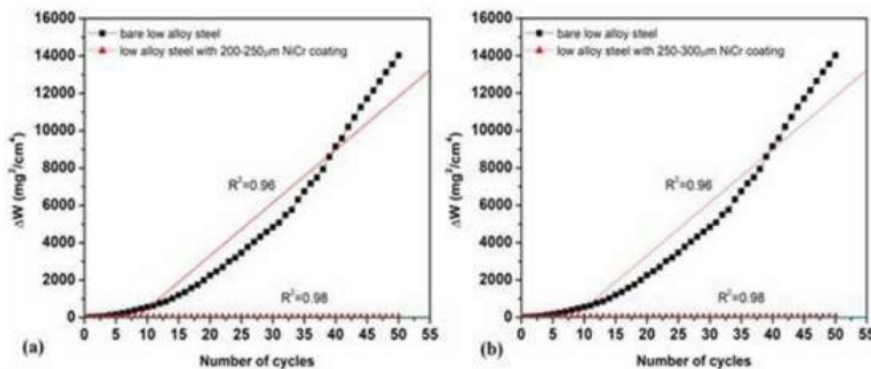


Figure 4. Weight gain square (mg^2/cm^4) vs number of cycles graph of (a) bare and 200-250 μm thick, and (b) bare and 250-300 μm thick, Ni-Cr coated low alloy steel subjected to high temperature oxidation.

It was observed that coated specimens followed parabolic rate law and show constant weight gain, thereby slowing down the further oxidation process. Initially higher weight gain was observed probably due to accelerated interfacial reaction. This weight gain may be due to the oxidation of entrapped air in the coating [3]. Elemental mapping of oxidized mild steel specimen shows Fe and O elements, which confirms the formation of iron oxides. Presence of Cr and O was confirmed by the needle/platelet type of oxides. Surface morphology of the coated specimen indicates a higher amount of Ni, Cr, and O, which may be attributed to the formation of nickel oxide and chromium oxide. Chromia provides resistance against oxidation at elevated temperatures, as it preferentially reacts with O_2 to form chromate and stabilizes the melt chemistry [10]. The presence of a thick continuous band of protective oxides in the scales of coated specimens does not allow the oxidizing species and the metallic ions to travel into the substrate and acts as a barrier to diffusion, resulting in the prevention of further oxidation processes.

4. CONCLUSIONS

1. Hardness of low alloy steel was increased from 202 to 342 VHN after the application of coatings.
2. Parabolic rate constant(K_p) for high temperature oxidation of bare, 200-250 μm , and 250-300 μm thick Ni-Cr coated low alloy steel were be 787.192, 0.235608, and 0.501787($\times 10^{-10} \text{g}^2 \text{cm}^{-4} \text{s}^{-1}$) respectively, The parabolic rate constant of coatings was found to be very small as compared to that of bare steel, indicating the protective nature of the coatings against high temperature oxidation.
3. 200-250 μm thick Ni-Cr coated steel showed better resistance against high temperature oxidation as compared to 250-300 μm thick Ni-Cr coated low alloy, because bond strength decreases with increase in coating thickness thereby corrosive media penetrates higher coating thicknesses easily as compared to lower coating thicknesses.

5. ACKNOWLEDGEMENT

At this moment of accomplishment, first of all I would like to show deep sense of gratitude to my guide Mr. Shivam Trivedi. This work would not have been possible without his guidance, support and encouragement. Under his guidance I successfully overcame many difficulties and learned a lot. Despite of all difficulties, he used to review my thesis progress, give his valuable suggestions and made corrections. His unflinching courage and conviction will always inspire me, and I hope to continue to work with his noble thoughts. I am also thankful to the faculty member of IIT Kanpur for providing required facilities for my research work.

6. REFERENCES

- [1] Khanna A.S., (2002), *Introduction to high temperature oxidation and corrosion*, ASM International, Materials Park, Ohio.
- [2] Sidhu T.S., Prakash S. and Agrawal R.D., (2006), *Studies of the metallurgical and mechanical properties of high velocity oxy-fuel sprayed stellite-6 coatings on Ni- and Fe-based superalloys*, *Surface Coat. Tech.*, Vol. 201(1), pp. 273-281.
- [3] Murthy J. K. N. and Venkataraman B., (2006), *Abrasive wear behaviour of WC-CoCr and Cr₃C₂-20(NiCr) deposited by HVOF and detonation spray processes*, *Surface Coat. Tech.*, Vol. 200(8), pp. 2642-2652.
- [4] Hocking M.G., (1993), *Coatings resistant to erosive/corrosive and severe environments*, *Surface Coat. Tech.*, Vol. 62(1-3), pp. 460-466.
- [5] Cvijovic I., Jovanovic M.T. and Perusko D., (2008), *Cyclic oxidation behaviour of Ti₃Al-based alloy with Ni-Cr protective layer*, *Corros. Sci.*, Vol. 50(7), pp. 1919-1925.
- [6] Bala N., Singh H. and Prakash S., (2009), *High temperature oxidation studies of cold sprayed Ni-20Cr and Ni-50Cr coatings on SAE 213-T22 boiler steel*, *App. Surface Sci.*, Vol. 255(15), pp. 6862-6869.
- [7] Rajput S. K., Dikovits M., Chaudhari G. P., Poletti C., Warchomicka F., Pancholi V., and Nath S. K., (2013), *Physical simulation of hot deformation and microstructural evolution of AISI 1016 steel using processing maps*, *Mater. Sci. Eng. A*, Vol. 587, pp. 291-300.
- [8] Rajput S. K., Chaudhari G. P., and Nath S. K., (2014), *Physical simulation of hot deformation of low-Carbon Ti-Nb microalloyed steel and microstructural studies*, *J. Mater. Eng. Perfor.*, Vol. 23 (8), pp. 2930-2942.
- [9] Rajput S. K., Chaudhari G. P., and Nath S. K., (2016), *Characterization of hot deformation behavior of a low carbon steel using processing maps, constitutive equations and Zener-Hollomon parameter*, *J. Mater. Proc. Tech.*, Vol. 237, pp. 113-125.
- [10] Kamal S., Jayaganthan R. and Prakash S., (2010), *High temperature cyclic oxidation and hot corrosion behaviours of superalloys at 900°C*, *Bull. Mater. Sci.*, Vol. 33(3), pp. 299-306.

Simulation of MHO Characteristics for Transmission Line Protection using PSCAD

Yashasvi B*, Vidushi K*, Ramesh P*

*Department of Electrical and Electronics Engineering, College of Engineering Roorkee, Roorkee, Uttarakhand, India.

ABSTRACT

Modeling of protective relays offer an economical and feasible alternative to investigate the performance of relays and protection systems. In this paper MHO characteristics and Bergeron model type transmission line are modelled and simulated using PSCAD/EMTDC software. To study the performance of the relay characteristics, single line to ground fault at different locations with various fault resistances are considered. A Fast Fourier Transform block in PSCAD/EMTDC has been used to extract the fundamental component. The test network used in this paper is 220kv transmission line system.

Keywords: Modeling, MHO relay, PSCAD/EMTDC.

I. INTRODUCTION

When a short-circuit fault occurs on a transmission line, distance relays gives protection and trips the circuit breaker by disconnecting the faulty portion from the healthy section. To study the behavior of a distance relay during short-circuits, for designing new prototypes, to check and optimize the performance of relays that already installed in power system, to design new relaying algorithms and to check the performance of the new relay equipment it is necessary to model the distance relay. Relay models helps engineers and consultants to select the relay types suited for a particular application and to analyze the performance. Researchers use relay model to investigate and improve protection design and algorithms. Instead of using actual prototypes, manufacturers use relay models to expedite and economize the process of developing new relays. Electric power utilities use relay models to confirm how the relay would perform during systems disturbances and normal operating conditions and to make the necessary corrective adjustment on the relay settings. The software models could be used for training young and inexperienced engineers and technicians. Thus, Computer models of relays permit investigators to observe in a very detailed way the performance in each internal module of the relay [1-2].

The first transient model of a distance relay was presented in [3], where the ninth-order state space mathematical model of a mho element was developed. Wilson and Nordstrom [4] modeled one measuring unit of a distance digital relay using MODELS of EMTP.

The input filter, analog-to-digital converter, fundamental frequency phasor calculator and relay measuring principle were modeled separately in MODELS. The simulations were compared with laboratory test results. A. A Abdrahem and H.H Sherwali, [5] described distance relay model using MATLAB environment and the behavior of the distance relay model verified by the Electromagnetic Transient Program. The Electromagnetic Transient Program (EMTP) was the first software that simulates the transient nature of power system [6] which is based on the algorithm proposed in [7]. PSCAD/EMTDC software is an electromagnetic transient analysis program developed by the Manitoba HVDC Research Center having variety of steady state and transient power system studies [8]. The primary solution engine is EMTDC, which solves equations for the entire power system in time domain employing the electromagnetic transient algorithm proposed in [7]. PSCAD is graphical user interface, provides powerful means of visualizing the transient behavior of the systems. PSCAD/EMTDC provides a fast and accurate solution for the simulation of electrical power systems [9].

In this paper, simulation of mho characteristics using PSCAD/EMTDC software has been proposed. The modeling is done by taking voltage and current signals at relay location and apparent impedance is calculated after extracting the fundamental component using Fast Fourier Transform block in PSCAD/EMTDC.

To study the performance of the developed characteristics single line to ground fault over the transmission line at different locations and different fault resistances are considered. The transmission line has been represented using the Bergeron line model in PSCAD/EMTDC.

II. DISTANCE RELAYS

A. Impedance seen by the distance relays

Distance relays are designed to protect power systems against four basic types of faults LG, LL-G, LL, and three phase fault. In order to detect any of the above faults, each one of the zones of distance relays require six units. Three units for detecting faults between the phases and the remaining three units for detecting phase to earth faults. The setting of distance relays is always calculated on the basis of the positive sequence impedance. Table. I indicate fault impedance calculation formula for all of the fault types.

Table I: Fault impedance calculation on different faults

Distance Element	Formula
Phase A	$Z_A = V_A / (I_A + 3kI_0)$
Phase B	$Z_B = V_B / (I_B + 3kI_0)$
Phase C	$Z_C = V_C / (I_C + 3kI_0)$
Phase A – Phase B	$Z_{AB} = V_{AB} / (I_A - I_B)$
Phase B – Phase C	$Z_{BC} = V_{BC} / (I_B - I_C)$
Phase C – Phase A	$Z_{CA} = V_{CA} / (I_C - I_A)$

Where, $k = (Z_0 - Z_1) / Z_1$, Z_0 and Z_1 are zero sequence and positive sequence impedances.

B. Zones of Protection

Distance relays will have instantaneous directional zone 1 protection and one or more time delayed zones. The tripping signal produced by zone 1 is instantaneous; it should not reach as far as the busbar at the end of the first line so it is set to cover only 80-85 per cent of the protected line. The remaining 20-15 percent provides a factor of safety in order to mitigate against errors introduced by the current and voltage transformers, and line impedance calculations. The 20-15 percent at the end of the line is protected by zone 2, which operates in t_2 seconds. Zone 3 provides the back-up and operates with a delay of t_3 seconds. Three protection zones in the direction of the fault are used in order to cover a section of line and to provide back-up protection to remote sections. Some relays have one or two additional zones in the direction of the fault plus another in the opposite sense, the latter acting as a back-up to protect the busbars. In the majority of cases the setting of the reach of the three main protection zones is made in accordance with the following criteria: Mho relay characteristics for three zones of protection as shown in the Fig. 1

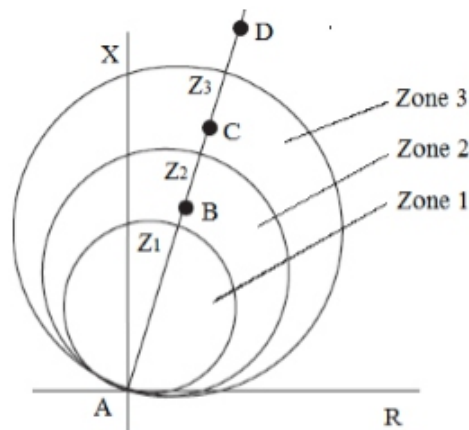


Fig. 1. Mho relay characteristics for three zones of protection.

Relay is located at A. Z_1 , Z_2 and Z_3 are the setting impedance of the mho relay for zone1, zone2 and zone3. AD is the total transmission line impedance divided into three zones AB, BC and CD.

Zone 1: This is set to cover between 80 and 85 per cent of the length of the protected line;

Zone 2: This is set to cover all the protected line plus 50 per cent of the shortest next line

Zone 3: This is set to cover all the protected line plus 100 per cent of the second longest line, plus 25 per cent of the shortest next line.

It is clear that the operating time of the relay is not the only factor to be considered while selecting a distance protection for transmission line applications.

C. Effect of fault Resistance on relay coverage

The reach of the mho relay effected in spite of the presence of fault resistance as shown in the Fig. 2. AB is the line to be protected, due to fault resistance BC impedance seen by the relay going out of the zone. Therefore mho relay under reaches because of fault resistance.

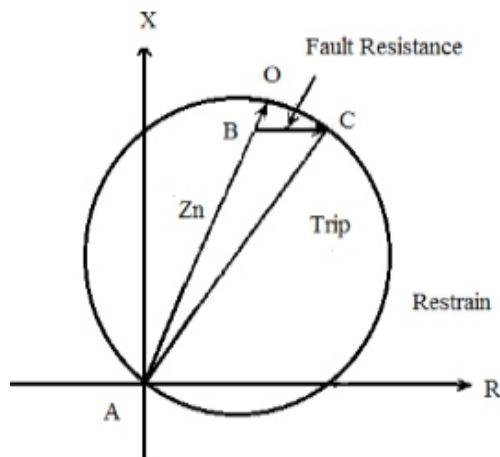


Fig. 2. Effect of fault resistance on reach of the relay.

III. MHO RELAY MODEL ALGORITHM

When a transmission line subjected to a fault, the voltage signals and current signals contain decaying dc components, higher order frequency components and lower order frequency components. The higher order frequency components can be eliminated using low pass anti-aliasing filters with appropriate cut-off frequency, but the anti-aliasing filters cannot remove decaying dc components and rejects lower order frequency components. This affects the performance of digital relay. Therefore, the Discrete Fourier transform is usually used to remove the dc-offset components [10]. The Fast Fourier Transform is a fast algorithm for efficient computation of DFT. FFT reduces the number of arithmetic operations and memory required to compute the DFT. Fig. 3 shows mho relay modeling algorithm, which uses FFT block in PSCAD/EMTDC for extracting the fundamental frequency component.

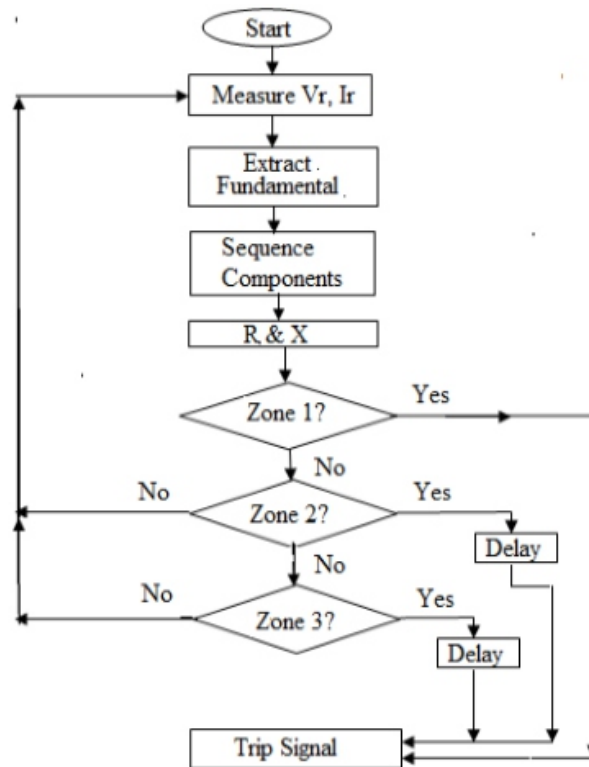


Fig. 3. Mho relay modeling Algorithm

IV. TRANSMISSION LINE MODEL

A Single line diagram of the transmission line operating at 220kV 50 Hz is shown in Fig. 4. The transmission line has been represented using the Bergeron line model in PSCAD/EMTDC software. Relay is located at bus-A. The data for the transmission line system is given in Appendix [1].

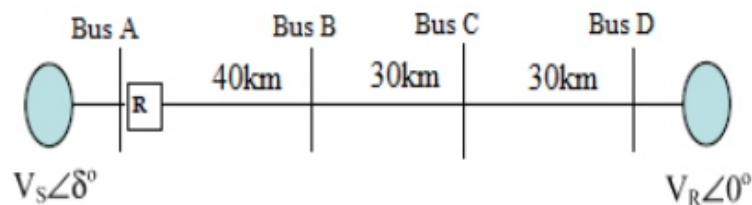


Fig. 4. Single line diagram of Transmission line.

Setting of the mho relay is

Zone-1 = 29.07 Ω (80 % of protected line AB).

Zone-2 = 49.97 Ω (100 % of protected line AB + 50 % of the protected line BC).

Zone-3 = 70.41 Ω (100 % of protected line AB + 100 % of the protected line BC + 25% of the protected line CD).

Impedance settings for the three zones are given in Table II.

Table II: Settings of Zones of Protection

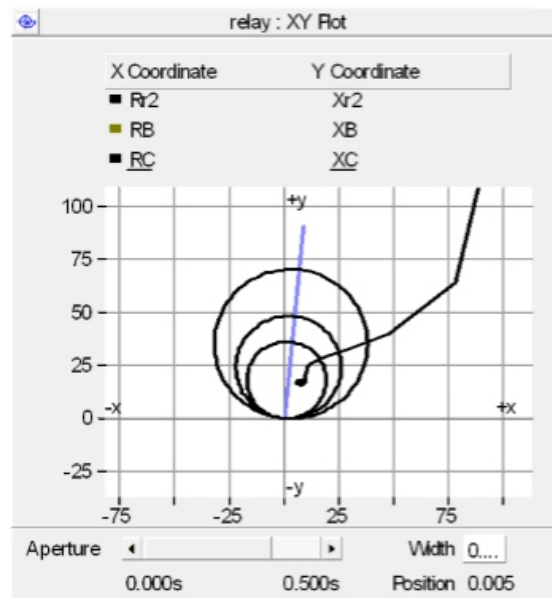
Zone	R	X
1	3.098 Ω	28.908 Ω
2	5.325 Ω	49.687 Ω
3	7.504 Ω	70.013 Ω

V. SIMULATION RESULTS

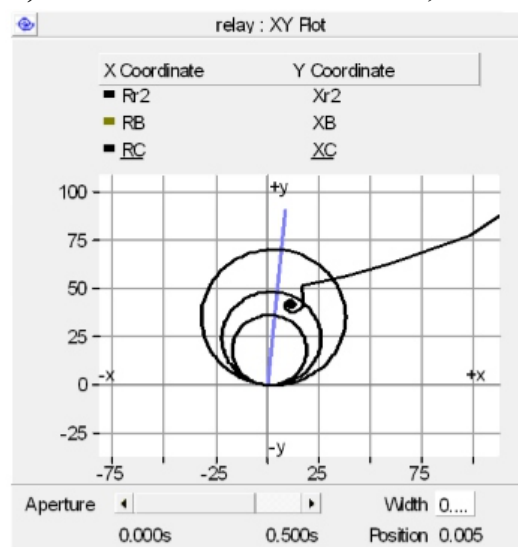
To study the behaviour of the developed mho relay characteristics, fault at different locations on the 220kv, 100km transmission line and fault resistances of different values were simulated using PSCAD/EMTDC software. The behaviour of of the mho relay is as explained hereinafter.

Case 1: - L-G faults at different distances from the relay location.

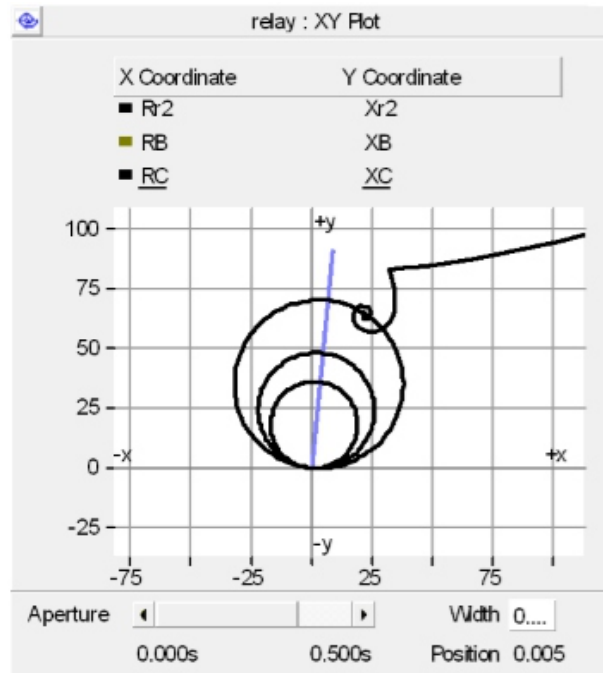
Single line to ground fault were set on the 220kv, 100 km transmission line model at a distance of 30km, 10km and 6 km from the location of bus-A, bus-B and bus-C. Simulation results are shown in Fig. 5a, 5b and 5c.



a) Fault At 30 Km from Bus-A, Zone 1



b) Fault at 10 km from Bus-B, Zone 2

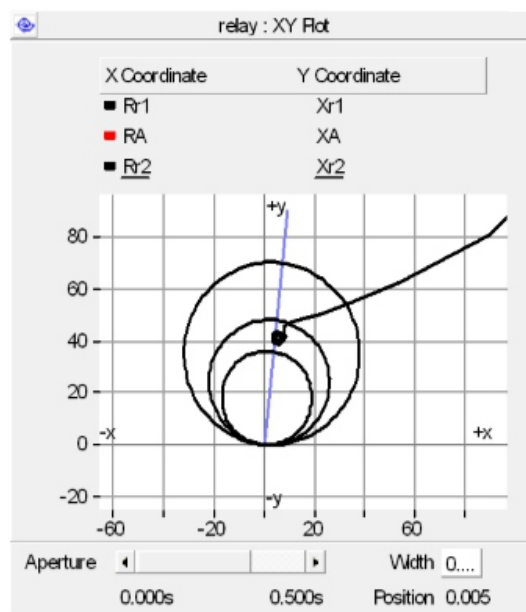


c) Fault at 6 km from Bus-C, Zone 3

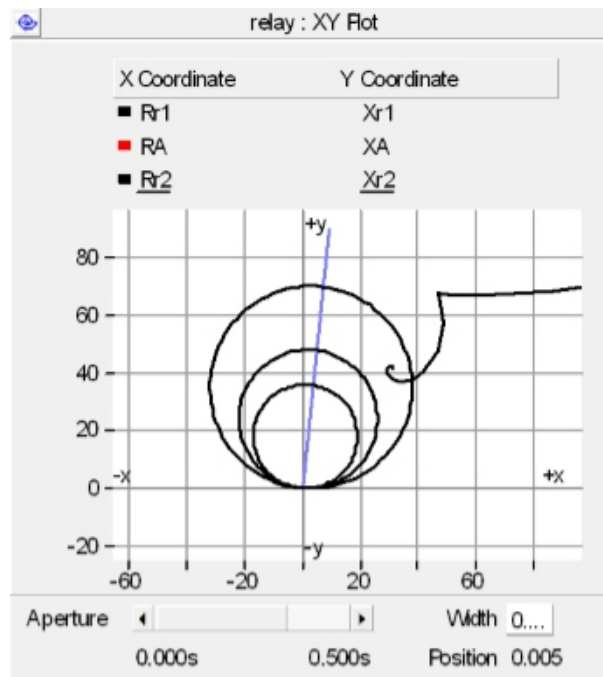
Fig. 5. Impedance trajectory of the relay for LG fault at different locations, case 1.

Case 2: Single line to ground fault with fault resistance

Single line to ground fault with different fault resistance were applied on the transmission line at a location 10 Km from bus-B, zone 2 with different fault resistances. Fig. 6.a and 6.b shows the behavior of the mho relay when fault resistance is 1 Ω and 18 Ω. When the fault resistance is 1 Ω the relay detects the fault in zone 1. Due to increase in fault resistance from 1 Ω to 18 Ω, impedance seen by the relay lies in the zone3 as shown in the Fig 6.b. Thus, mho relay under reaches due to fault resistance.



(a) Fault resistance of 1Ω



(b) Fault resistance of 18Ω

Fig. 6. Impedance trajectory of the relay for LG fault with different fault resistances, case 2.

VI. CONCLUSIONS

In this paper mho relay characteristics are developed using PSCAD. The performance characteristics of mho relay was evaluated at different locations with single line to ground fault. Main conclusion of this work is as follows.

- The developed mho characteristics may be used for training young and inexperienced engineers and technicians.
- Different case studies have been presented in order to illustrate the response of the developed mho characteristics at different locations and different fault resistances. Resistive fault causes the relay to under-reach.

APPENDIX

Source Data at both Sending and Receiving Ends positive –sequence impedance = $0.819+j7.757 \Omega$ zero sequence impedance = $3.681+j24.515 \Omega$ frequency = 50Hz

Transmission line data

voltage = 220kV

positive sequence impedance = $0.09683+j0.903 \Omega/\text{km}$ zero sequence impedance = $0.01777+j0.4082 \Omega/\text{km}$ frequency = 50Hz

REFERENCES

1. Hamid Sherwali and Abdraham, *Matlab - Modelling, Programming and Simulations*, InTech publishers, October 2010.
2. Abdlmnam A. Abdraham, "Modeling of distance relays for Power Systems Protection", M.Sc. dissertation, EE&E Dept., Faculty of Engineering, Al-Fatah University, Fall 2007.
3. Z. Peng, M. S. Li, C. Y. Wu, T. C. Cheng, and T. S. Ning, "A dynamic State Space Model of a Mho Distance Relay," *IEEE Transactions on Power Apparatus and Systems*, Vol. PAS-104, No. 12, December 1985.
4. R. E. Wilson, J. M. Nordstrom, "EMTP Transient Modeling of a Distance Relay and a Comparison with EMTP Laboratory Testing," *IEEE Transactions on Power Delivery*, Vol. 8, No. 3, July 1993.
5. A.A Abdraham and H.H Sherwali, "„Modeling Of Numerical Distance Relays Using Matlab", *IEEE Symposium on Industrial Electronics and Applications ISIEA*, October 2009.
6. H. Dommel, "EMTP Reference Manual," *Bonneville Power Administration* 1986.
7. H. W. Dommel, "Digital Computer Solution of Electromagnetic Transient in Single- and Multiphase Networks," *IEEE Transactions on Power Apparatus and Systems*, Vol. PAS-88, No. 4, April 1969.
8. *Introduction to PSCAD/EMTDC V3*, Manitoba HVDC Research Centre Inc., Canada, 2000.
9. Craig Muller, P. Eng. "Power system computer aided design user"s guide", *Manitoba HVDC Research Centre*, September 2005
10. Abdlmnam A. Abdraham, Hamid H Sherwali, "Modelling of Numerical Distance Relays Using Matlab", *IEEE Symposium on Industrial Electronics and Applications*, Kuala Lumpur, Malaysia, October 4-6, 2009.

Design of Morphological Approach to Detect and Eliminate Ink Bleed in Document Images

Kusum Grewal *, Renu Malhan **

Mechanical Engineering Department, Faculty of Engineering and Technology, Rama University,
Kanpur, Uttar Pradesh, India

Assistant Professor, Mechanical Engineering Department, FET, Rama University, Kanpur, Uttar
Pradesh, India

ABSTRACT

When we write some text on a paper either hand written or the printed it gives the impression of text on its back side. More the ink pressure more dark will be the impression on back side. Now if we write the text on this impression side it is not readable clearly. In case of scanned copy of such documents there is the problem to read the documents as well as to extract the actual text from this. This back side impression of the text is called ink bleed. Ink bleed is one of the major problems while reading the older documents or the manuscripts. In this proposed work we are presenting the way to resolve the problem of ink bleed. Here the research is being performed using the morphological operators to detect and eliminate the ink bleed from a ink-bleeded document.

Keywords: Ink Bleed, Manuscript, Morphological Operators, Elimination, Detection.

I. INTRODUCTION

The objective of document image processing is to recognize text and graphics components in images of documents, and to extract the intended information as a human would. Two categories of document image processing can be defined:

A) Textual processing deals with the text components of a document image. Some tasks here are: determining the skew (any tilt at which the document may have been scanned into the computer), finding columns, paragraphs, text lines, and words, and finally recognizing the text (and possibly its attributes such as size, font etc.) by optical character recognition (OCR). Graphics processing deals with the non-textual line and symbol components that make up line diagrams, delimiting straight lines between text sections, company logos etc. Pictures are a third major component of documents.

Document analysis systems will become increasingly more evident in the form of everyday document systems. For instance, OCR systems will be more widely used to store, search, and excerpt from paper-based documents. Page-layout analysis techniques will recognize a particular form, or page format and allow its duplication. Diagrams will be entered from pictures or by hand, and logically edited. Pen-based computers will translate handwritten entries into electronic documents. Archives of paper documents in libraries and engineering companies will be electronically converted for more efficient storage and instant delivery to a home or office computer. Though it will be increasingly the case that documents are

produced and reside on a computer, the fact that there are many different systems and protocols, and also the fact that paper is a very comfortable medium for us to deal with, ensures that paper documents will be with us to some degree for many decades to come. The difference will be that they will finally be integrated into our computerized world.

B) Ink-bleed through Housed within the libraries of the world is a great collection of rare books and handwritten manuscripts. The information contained in these collective works was often unavailable to most people. Due to this sometimes high expense of time and money required to travel to the locations in which documents of interest were stored. With the recent advent of the Internet, or more specifically, the growth in computer and telecommunications technology, it is now possible to create online digital libraries enabling most people around the world to potentially access any document anywhere. These digital libraries help in:

- Preserving important information for decades
- Reproduction
- Distribution
- Retrieval
- Analysis

The first step in creating a digital library is to get the documents into digital format. The most popular method of digitizing any picture is to have it scanned. These scanned documents usually suffer from much degradation that can occur either during scanning or because of physical conditions.

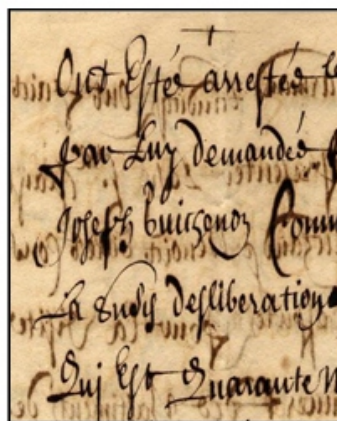


Figure 1 : Examples of ink-bleed through.

This thesis work concentrates on physical degradation that is “Ink-bleed through”. This degradation is due to ink’s seeping through the pages of documents after long periods of storage. The result is that characters from the reverse side appear as noise on the front side. Indeed, the content of the original side is combined with the content of the reverse side (Fig 1.2). This can deteriorate the legibility of the

document if the interference acts in a significant way. The severity and characteristics of ink-bleed is related to a variety of factors including the ink's chemical makeup, the paper's physical and chemical construction, the amount of ink applied and the paper's thickness (both spatially varying), the document's age, and the amount of humidity in the environment housing the documents.

QUANTITATIVE MEASURES

Ink-bleed through removal of a document image is carried out to enhance its readability and to get a clean image by using any of ink-bleed through removal approaches so that these images can be further used for reading or for OCR. It helps in performing segmentation in OCR as it is mainly used for pre-processing of an image. The quality of ink-bleed through removal algorithm is measured by using the following quantitative measures:

1. Precision: It shows how well the system can remove the interfering strokes. It can be evaluated as:

$$\text{Precision} = \frac{\text{No. of words correctly detected}}{\text{Total no. of words detected}}$$

2. Recall: It is a measure of the performance of the system in restoring the front page to its original state.

It can be evaluated as:

$$\text{Recall} = \frac{\text{No. of words correctly detected}}{\text{Total no. of words in the document}}$$

3. F-Measure: A measure that combines precision and recall, it is the harmonic mean of precision and recall, the traditional F-measure or balanced F-score:

$$F = 2 \frac{\text{precision} \times \text{recall}}{\text{precision} + \text{recall}}$$

This is also known as the F1 measure, because recall and precision are evenly weighted. It is a special case of the general F_β measure (for non-negative real values of β):

$$F_\beta = (1 + \beta^2) \frac{\text{Precision} * \text{Recall}}{\beta^2 * \text{Precision} + \text{Recall}}$$

Two other commonly used F measures are the F2 measure, which weights recall higher than precision, and the F0.5 measure, which puts more emphasis on precision than recall.

The obvious drawback of ink-bleed is the reduction in the document's legibility. The motivation of our work is to provide a practical approach to reduce ink-bleed interference in imaged documents in order to improve legibility.

II. LITERATURE SURVEY

Huang Y. et al. [1], presented a novel user-assisted approach for Ink-bleed through removal found in old manuscripts. The problem is addressed by first having the user provide simple examples of foreground ink, Ink-bleed, and the manuscript's background. From this user-labeled data, each pixel is classified as foreground, Ink-bleed, or background and used as the data costs of a dual-layer Markov random field (MRF) that simultaneously labels all pixels in both the front and back sides of the manuscript. This user-assisted approach produces better results than existing algorithms without the need for extensive parameter tuning or prior assumptions about the Ink-bleed intensity characteristics. Overall application framework was discussed along with details of the features used in the data costs, a comparison between K-nearest neighbour and support vector machine for likelihood estimation, the dual-layer MRF formulation with associated inter- and intra-layer costs, and a comparison of this approach against other ink-bleed reduction algorithms. Overall procedure that was adopted is as follows:

- 1) Image alignment with local refinement;
- 2) Training-data collection via minimal user-assistance;
- 3) Pixels labelling using the dual-layer MRF framework;
- 4) Output image generation.

The results demonstrate that DL-MRF-SVM and DL-MRF-KNN approaches can generate results superior to previous approaches.

Wolf C. [2], presented a method for blind document bleed through removal based on separate Markov Random Field (MRF) regularization for the recto and for the verso side, where separate priors were derived from the full graph. The segmentation algorithm is based on Bayesian Maximum a Posteriori (MAP) estimation. He concentrated on ink bleed through removal, i.e. the separation of a single scanned document image, into a recto side and a verso side. The novelty of the method is the separation of the MRF prior into two different label fields, each of which regularizes one of the two sides of the document. This separation allows to estimate the verso pixels of the document which are covered by the recto pixels, which, again through the MRF prior, improves the estimation of the verso pixels not covered by recto pixels, thus increasing the performance of the regularization. He showed that this formulation leads to an efficient algorithm based on graph cuts.

The performance of the method has been evaluated on scanned document images from the 18th century, showing that the restoration is able to improve the recognition performance of an OCR significantly, compared to non-restored images but also compared to competing methods.

Moghaddam R. et al. [3], adapted the variational model by using an estimated background according to the availability of the verso side of the document image. In this approach, based on the availability of the verso side, different models have been developed which can be applied to document images degraded by bleed-through. The first model they present is variational model for restoration of double-sided document images. Then for restoration without the verso side image, a modified variational model is introduced which removes the interference patterns using the estimated background information. For document images containing very fine features and structures, the second model is modified to include a global classifier, the flow field, which helps preserving these very weak edges, while at the same time achieving a high degree of smoothing and enhancement. This is called global control or flow field. The solution of each resulting model was obtained using wavelet shrinkage or a time-stepping scheme, depending on the complexity and nonlinearity of the models. When both sides of the document are available, the proposed model uses the reverse diffusion process for the enhancement of double-sided document images. The results of experiments with real and synthesized samples are promising. The proposed model, which is robust with respect to noise and complex background, can also be applied to other fields of image processing. The performance of the models was evaluated against other methods, such as the ICA method, in both subjective and objective ways using several databases of different types of document script and degradation.

Tonazzini A. et al. [4], proposed a system to process multispectral scans of double-sided documents. It can co-register any number of recto and verso channel maps, and reduce the bleed-through/show-through distortions by exploiting blind source separation. From RGB scans, it is also able to recover the original colors, thus improving the readability of a document while maintaining its original appearance. The recto and verso patterns obtained can then be further analyzed. The aim is twofold: to produce enhanced versions of all the available scans at the different wavelengths, and a restored visible document that, while cleansed of the unwanted interferences, maintains its useful features as much as possible. This approach mainly consists of two steps:

- 1) Registration of multispectral scans of recto- verso pairs
- 2) Removing interference from registered data

Experimental results show that for RGB reconstructions of two RGB recto-verso scans, a significant attenuation of the bleed-through has been obtained, and the original color has been pretty well recovered. The RGB recto and verso images thus obtained can further be analyzed to extract possible extra uncorrelated patterns. The overall procedure could constitute a fast, reliable and effective system to be routinely used in libraries and archives for the enhancement of multispectral scans of degraded documents. The method is flexible for use in various contexts of document analysis, such as the extraction of hidden or masked patterns.

III. PROPOSED WORK

A morphological operator is therefore defined by its structuring element and the applied set operator. For the basic morphological operators the structuring element contains only foreground pixels (i.e. ones) and 'don't care's'. These operators, which are all a combination of erosion and dilation, are often used to select or suppress features of a certain shape, e.g. removing noise from images or selecting objects with a particular direction.

In erosion, every object pixel that is touching a background pixel is changed into a background pixel. In dilation, every background pixel that is touching an object pixel is changed into an object pixel. Erosion makes the objects smaller, and can break a single object into multiple objects.

Dilation makes the objects larger, and can merge multiple objects into one. As shown in (d), opening is defined as an erosion followed by a dilation. Figure (e) shows the opposite operation of closing, defined as a dilation followed by an erosion. As illustrated by these examples, opening removes small islands and thin filaments of object pixels. Likewise, closing removes islands and thin filaments of background pixels.

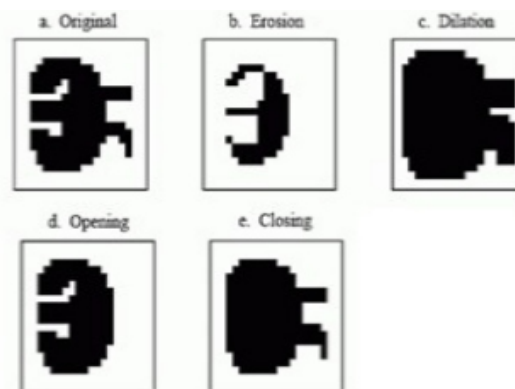


Figure. 2 Morphological operations. Four basic morphological operations are used in the processing of binary image: erosion, dilation, opening and closing. Fig (a) shows an example binary image. Fig (b) to (e) shows the result of applying these operations to the image in (a).

The proposed architecture is given as figure 3.

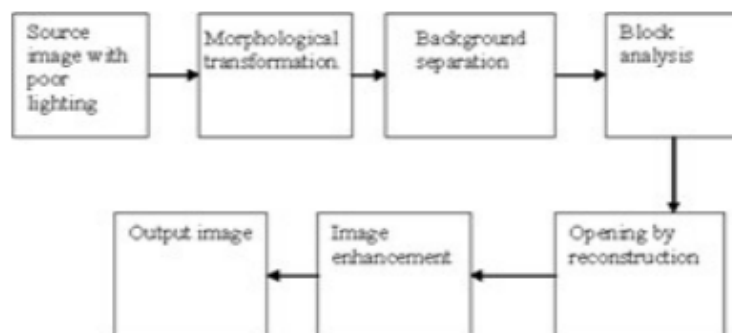


Figure 3 : Proposed Architecture

This method is introduced to overcome the limitation of thresholding in Blind segmentation approach. The proposed algorithm is as follows:

ALGORITHM

Step 1: Read the input image degraded from ink-bleed through.

Step 2: Apply the morphological operations like Erosion, Dilation, Opening, Closing on the source image.

Step 3: Perform the block analysis on the image to find the blocks of different intensity level and that requires the enhancement.

Step 4: Reconstruct the blocks separately.

Step 5: Perform Image Enhancement. The lighter part will be dissolve and the darker is left

Step 6: Increase the contrast of remaining image. Step 7: Show the Restored output image.

IV. CONCLUSION

Here a new algorithm is presented to remove the ink bleed impression from the document images. The morphological approach gives a segmented approach and it appear the results will be better and efficient then existing approaches.

REFERENCES

1. Y.Huang, M.S. Brown, and D. Xu, Member, IEEE, "User-Assisted Ink-Bleed Reduction", *IEEE transaction on image processing*, pp.2646-2658, vol.19, no. 10, October 2010.
2. C .Wolf, , "Document ink bleed-through removal with two hidden markov random fields and a single observation field", *IEEE transaction on pattern analysis and machine intelligence*, pp.431-447, vol.32, no.3, march 2010.
3. R. F. Moghaddam, M. Cheriet, Senior Member, IEEE, "A variational approach to degraded document enhancement", *IEEE transaction on pattern analysis and machine intelligence*, pp.1347-1361, vol. 32, no. 8, August 2010.
4. A. Tonazzini, G. Bianco, E. Salerno, "Registration and enhancement of double-sided degraded manuscripts acquired in multispectral modality", in *Proceedings of 10th International Conference on Document Analysis and Recognition*, 2009.
5. J. Wang, M. S. Brown, C. L. Tan, "Accurate Alignment of Double-Sided Manuscripts for Bleed-Through Removal," in *Proceedings of the eighth International Association for Pattern Recognition(IAPR) International Workshop on Document Analysis Systems*, pp.69-75, 2008.
6. C. Wolf, "Improving recto document side restoration with an estimation of the verso side from a single scanned page", in *Proceedings of international Conference of Pattern recognition (ICPR)*, pp.1-4, 2008.
7. A. Tonazzini, E. Salerno, and L. Bedini, "Fast correction of bleed through distortion in grayscale documents by a Blind Source Separation technique", *International Journal on Document Analysis and Recognition (IJ DAR)*, vol. 10, pp.17–25, June 2007.
8. R. D. Lins and J. M. M. da Silva, "Assessing Algorithms to Remove Back-to-Front Interference in Documents", in *Proceedings of ITS-2006, Fortaleza, Brazil*, IEEE Press, pp.868-873, 2006.
9. F. Drira, F. L. Bourgeois, and H. Emptoz, "Restoring ink bleed-through degraded document images using a recursive unsupervised classification technique", In *Document Analysis Systems*, pp.38–49, 2006.
10. F. Drira, "Towards Restoring Historic Documents Degraded Over Time," dial, in *Proceedings of Second International Conference on Document Image Analysis for Libraries (DIAL'06)*, pp.350-357, 2006.

-
11. R.C. Pinto, L. Bandeira, M.C. Sousa, P. Pina, "Combining Fuzzy Clustering and Morphological Methods for Old Documents Recovery", in *Proceedings of the Iberian Conference on Pattern Recognition and Image Analysis (IBPRIA)*, pp.387-394, 2005.
 12. Q. Wang, T. Xia, L. Li, C. L. Tan, "Document Image Enhancement Using Directional Wavelet," *IEEE Computer Society Conference on Computer Vision and Pattern Recognition (CVPR'03)*, vol. 2, pp.534, 2003.
 13. H. Nishida and T. Suzuki, "Correcting show-through effects on document images by multiscale analysis", in *Proceedings of the International Conference on Pattern Recognition(ICPR)*, vol. 3, pp.65–68, 2002.
 14. E. Dubois and A. Pathak, "Reduction of bleed-through in scanned manuscript documents", in *Proceedings of Image Capture Systems (PICS)*, pp.177–180, 2001.
 15. Q. Wang, C.L. Tan, "Matching of Double-Sided Document Images to Remove Interference," *IEEE Computer Society Conference on Computer Vision and Pattern Recognition (CVPR'01)*, vol. 1, pp.1084, 2001.
 16. K. Knox, "Show- Through Correction for Two-Sided Documents", *United States Patent 5,832,137*, Nov. 1998.

Thermal-Hydraulic Analysis of Fuel Rod of a TRIGA Mark II Research Reactor

Md. Shafiqul Islam¹, Abid Hossain Khan^{1,2*}

¹ Department of Nuclear Engineering, University of Dhaka, Dhaka-1000, Bangladesh

² Department of Industrial and Production Engineering, Jashore University of Science and Technology, Jashore-7408, Bangladesh

*Corresponding author E-mail: khanabidhossain@gmail.com

ABSTRACT

In this work, the feasibility of employing “Single Flow Channel Analysis” technique for obtaining the thermal-hydraulic behavior of a TRIGA Mark II research reactor has been studied. Two different simulation methods have been investigated for this purpose; one in which there is no variation in volumetric heat generation along the fuel axis and the other in which there is variation. A hot rod factor of 1.70 has been taken. Results obtained from simulation methods have been compared with both theoretical results and experimental data provided by the manufacturers. Results show that data generated from both simulation methods are more accurate compared to theoretical calculations. Also, the simulation method exempting variation of heat generation has predicted maximum temperature of the fuel centerline just above 750 oC, which is sufficiently accurate. However, temperatures obtained at different axial and radial locations are not close to the experimental values. On the other hand, the simulation technique in which variation of heat generation exists has been able to provide temperature profiles inside the fuel rod and cladding surface almost identical to the experimental values. However, temperature profile of the fuel outer surface is found to be quite different from experimental values.

Keywords: Hot Rod Factor; Research Reactor; Temperature Distribution; Thermal-Hydraulics.

1. INTRODUCTION

Unlike power reactors, research reactors are specially designed nuclear reactors that are to be used for research purpose only. While power reactors produce heat energy that may be converted to useful electric energy, research reactors produce radioactive rays or particles such as neutron, α , β and γ -rays, etc. These radioactive rays and particles are used for radioactive isotope production and other research works. Heat generated during the fission chain reaction in the core is nothing but a byproduct for these reactors [1]. Research reactor fuels usually have a higher enrichment of U-235 compared to power reactors. The enrichment of U-235 is just below 20%, which is the upper limit of low-enriched uranium (LEU) fuel. In case of power reactors, this value is usually below 5%. The excess enrichment is necessary because these reactors are designed to produce maximum amount of fast neutrons, unlike power reactors that have no use of fast neutrons. Also, a massive portion of this neutron is extracted from the reactor core for research purpose. As a result, the availability of thermal neutrons is less compared to power reactors, making it difficult to sustain chain reaction at enrichment limit just below 5%. However, enrichment level above 20% is not accepted in order to avoid proliferation risks [2].

TRIGA is a pool-type reactor that is designed for research and material testing use by scientific institutions and universities. It is mostly used for undergraduate and graduate education, private commercial research, non-destructive testing, and isotope production [3]. The TRIGA reactor uses Uranium Zirconium Hydride ($U_{0.3}Zr_{1.6}H$) fuel. It has a prompt negative fuel temperature coefficient of reactivity that results in decrease in reactivity with increase in core temperature [4]. Uranium Zirconium Hydride fuels can operate at a linear heat rate (LHR) of ~ 80 MW/m with a maximum fuel centerline temperature of 820 °C [5]. Another advantage of these fuels is that fission-gas release is quite small up to 600 °C for these fuels [6]. Since these fuels do not support high temperature operation in order to avoid swelling, inert Pb-Bi-Sn liquid metal is used in between the gap of fuel pellet surface and the inner surface of the cladding instead of helium for TRIGA fuels. This modification decreases the centerline temperature of the fuel significantly [7]. Finally, the thermal conductivity of Uranium Zirconium Hydride fuel is around 20 W/m.K, which is almost 7 times higher than Uranium Oxide fuel [8]. As a result, the centerline temperature remains much lower for TRIGA reactors than conventional nuclear power plants.

TRIGA Mark-II is one of the design variations of the TRIGA research reactor types. Till date, this model is operational in multiple countries. This reactor has been used for a variety of research works and scientific studies, both experimental and numerical. Žerovnik et al. studied the use of multiple detectors on the measurement of thermal power of a TRIGA Mark II research reactor [9]. Nacir et al. worked on the safety analysis and optimization of the core fuel reloading for TRIGA Mark-II reactor in Morocco [10]. Agbo et al. analyzed the thermal power calibration methods of the Nigerian research reactor [11]. Štancar and Snoj suggested an improved thermal power calibration method for TRIGA Mark II research reactor [12]. A combined experimental and numerical study is also common in the literature for TRIGA Mark II reactors. Coupling numerical simulation techniques with research reactor experimental studies can greatly reduce the cost to be incurred during research works. Cammi et al. suggested zero-dimensional model for simulating the dynamic response of TRIGA Mark II reactor [13]. El-Bakkari et al. conducted a fuel burnup analysis for TRIGA research reactor using Monte-Carlo nuclear code [14]. Türkmen and Çolak conducted a similar type of analysis [15]. Coban suggested a method for power level control of the TRIGA Mark-II reactor using the multi-feedback layer neural network and the particle swarm optimization [16]. Alloni et al used the Monte Carlo code for final characterization of the first critical configuration for TRIGA Mark II reactor of the University of Pavia [17]. Henry conducted a study on the physical parameters of JSI TRIGA MARK II reactor using TRIPOLI and MCNP [18]. Mghar calculated the kinetic parameters of the Moroccan TRIGA Mark-II reactor using the Monte Carlo code [19]. Cammi et al. did a characterization of the TRIGA Mark II reactor during a steady-state, full power operational condition [20]. Čalić et al. validated the Serpent 2 code on benchmark experiments of

TRIGA Mark II research reactor [21]. Henry et al. suggested a CFD/Monte-Carlo neutron transport coupling scheme applicable for TRIGA reactor [22].

The one and only research reactor in Bangladesh is the 3 MW TRIGA Mark II research reactor located at Atomic Energy Research Establishment (AERE), Savar, Dhaka. It was constructed and supplied by General Atomics, San Diego, California, USA. The reactor has been operational since 1986 [23]. Since the commissioning of the reactor, it has been an essential part of numerous nuclear research programs of Bangladesh Atomic Energy Commission (BAEC). Lyric et al. conducted an experimental study to obtain the optimum burnup of BAEC TRIGA research reactor [24]. Khan et al. analyzed the kinetic parameters of 3 MW TRIGA Mark-II research reactor at AERE using the SRAC2006 code [25]. Salam et al. measured the control rod reactivity and shutdown margin of the research reactor using analogue and digital I&C system [26]. Rahman et al. conducted a steady-state thermal-hydraulic analysis of the reactor [27]. Salam et al. measured the neutronic safety parameters of the reactor [28]. The study was extended later on by Hosan et al. [29]. Hoq et al. estimated Ar-41 activity concentration and its release rate from the reactor [30].

From the literature survey, it is evident that there have been quite a number of researches related to TRIGA Mark II research reactor. But to the best of the authors' knowledge, the prospect of using simulation tools for obtaining solely the thermal-hydraulic behavior of the fuel rod of this reactor might not have been studied earlier. Furthermore, the simplification of the simulation geometry by applying single flow channel analysis technique might not have been focused on with sufficient importance. In this work, an attempt has been made to find out the feasibility of using single flow channel analysis technique for simulating the thermal behavior of the fuel rod inside a TRIGA Mark II reactor core. In order to do so, the results from the simulation methods have been compared with results from theoretical analysis as well as experimental data.

2. METHODOLOGY

2.1. Governing equations for assessments of hydrodynamic characteristics

The 3MW TRIGA Mark II research reactor at AERE consists of 93 fuel elements, 6 control rods, 18 Graphite dummy elements, 1 Dry Central Trimble, 1 Rabbit Terminus and 1 neutron source. Again, the fuel rods are arranged in a hexagonal housing, which results in triangular array of the fuel rods. Fig.1 shows the arrangement of fuel rods in the core of the 3MW TRIGA Mark II research reactor at AERE, Savar. Since thermal-hydraulic simulation of such complex geometry will be very time consuming and complicated, it is more logical to go for single flow channel analysis. To do so, it is assumed that there

exists a single flow channel of annular shape that has the same hydraulic diameter as that of the triangular flow channel of the reactor. The equivalent hydraulic diameter of the flow channel for triangular array (see Fig.2a) may be deduced as,

$$D_h = \frac{4A_{cross}}{\text{wetted perimeter}} = d_{clad,out} \left[\frac{2\sqrt{3}}{\pi} \left(\frac{p}{d_{clad,out}} \right)^2 - 1 \right] \quad (1)$$

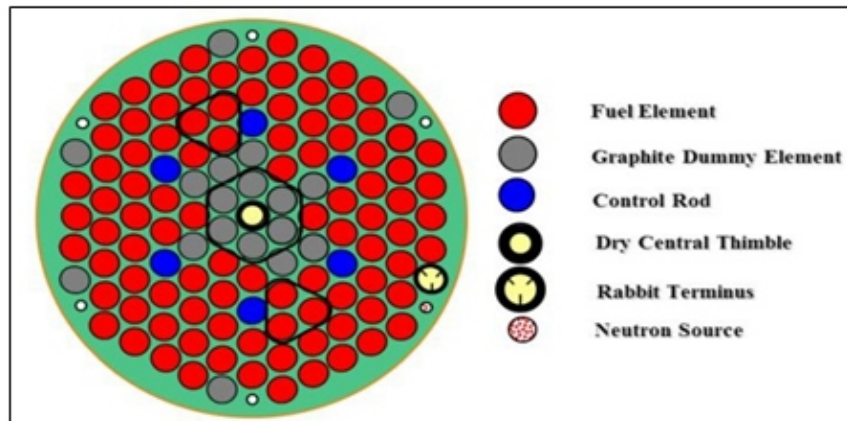


Fig. 1: Arrangement of Fuel Rods in 3MW TRIGA Mark II Reactor Core [23].

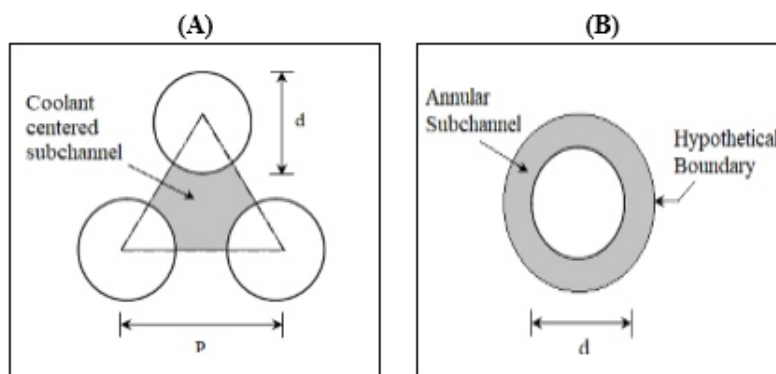


Fig. 2: A) Triangular Flow Channel, B) Annular Flow Channel.

Here $d_{clad,out}$ is cladding outer diameter, A_{cross} is cross-sectional area of flow sub-channel and p is pitch of the triangular array. For TRIGA Mark II reactor at AERE, this hydraulic diameter is calculated to be around 1.93cm.

It may be noted that for single channel flow analysis, it has been assumed that the coolant flows through an annular space between the outer surface of the cladding and a hypothetical boundary, as shown in Fig.2b. The diameter of the outer hypothetical boundary should be such that the hydraulic diameter of the annular flow channel remains the same. As a result, the diameter of the hypothetical boundary of the flow channel is calculated to be around 4.598 cm for TRIGA Mark II research reactor.

The total pressure drop across the reactor core in axial direction may be given by,

$$\Delta P_t = (P_{out} - P_{in}) = \Delta P_{friction} + \Delta P_{elev} + \Delta P_{entry} + \Delta P_{exit} \quad (2)$$

Here, $\Delta P_{\text{friction}}$ is frictional pressure drop, ΔP_{elev} is pressure drop due to elevation, ΔP_{entry} is pressure drop in the entry region and ΔP_{exit} is pressure drop at the exit region. Equation (2) may be re-written as,

$$\Delta P_t = \rho g H - \left\{ f \left(\frac{L}{D_h} \right) + K_{\text{in}} + K_{\text{out}} \right\} \rho \frac{v^2}{2} \quad (3)$$

Here, ρ is density of the coolant water, H is the height of the flow channel, f is friction factor, v is velocity of the coolant and K is kinetic head loss coefficient. In case of TRIGA fuel, the cladding outer surface is very smooth. As a result, frictional head loss is very negligible. Also, pressure drop due to elevation is very small. Therefore, pressure drop observed in the flow channel is basically the sum of the pressure drops at the entry and exit location of the coolant.

2.2. Governing equations for assessments of thermal characteristics

In a nuclear power reactor, the sole purpose of the nuclear chain reaction is production of thermal energy which may be converted to electricity. On the other hand, a research reactor is designed for producing radioactive rays and particles for research purpose. The heat produced is nothing but a byproduct and has no use whatsoever. Nevertheless, the heat energy produced in any of the two types of reactors needs to be removed from the core to avoid heating and subsequent meltdown. The rate of heat generation in a nuclear reactor may be given by,

$$\dot{q} = GN\sigma_f V_F \phi_{\text{avg}} \quad (4)$$

Here \dot{q} is heat generation rate (W), G is energy produced per fission (J/ fission), N is number of fissionable fuel nuclei/ unit volume (atoms /cm³), σ_f is microscopic fission cross-section of the fuel (cm²), V_F is volume of the fuel (cm³) and ϕ_{avg} is average neutron flux (n/cm².s) inside the core.

Unlike a power reactor, the heat produced in the core is removed by the coolant only to be dumped to the atmosphere. The rate of heat removal should, therefore, be equal to the rate of heat generation and is given by,

$$\dot{q} = \dot{m} C_{p,c} \Delta T \quad (5)$$

Here \dot{m} is mass flow rate (kg/s), $C_{p,c}$ is specific heat capacity of reactor coolant (J/ kg °K) and ΔT is temperature difference across the reactor core (°C).

For most types of reactors except boiling reactor, the temperature of the coolant is dependent upon reactor power and coolant flow rate as seen in Eq. (3). If flow rate is constant, temperature will vary directly with reactor power. If reactor power is constant, temperature will vary inversely with flow rate. Since the rate of heat generation is ideally proportional to the volume of the fuel, it is far more convenient to use volumetric heat generation rate rather than the overall rate of heat generation. The average value of volumetric heat generation may be given by,

$$\dot{q}'''_{avg} = \frac{\dot{q}}{V_F} \quad (6)$$

In case of TRIGA Mark II research reactor established in Atomic Energy Research Establishment (AERE) under the Bangladesh Atomic Energy Commission, the average volumetric heat generation rate is found to be $\sim 75.8 \text{ MW/m}^3$.

The volumetric heat generation rate at any axial location is given by,

$$\dot{q}''' = q_{max}''' \cos\left(\frac{\pi z}{H}\right) \quad (7)$$

Here z is the location at axial direction. Volumetric heat generation rate at a specific location of the fuel element is proportional to the neutron flux at that location. Since neutron flux varies in the axial direction of the fuel rod, volumetric heat generation rate also varies in the axial direction. The expression for volumetric heat generation rate related to neutron flux is presented in equation (8).

$$\dot{q}'''(z) = \dot{q}'''_{avg} \frac{\varphi(z)}{\varphi_{avg}} \quad (8)$$

Here is the volumetric heat generation rate at any axial distance z and is neutron flux at that location. Also, heat flux is proportional to volumetric heat generation. As a result, the distribution of neutron flux inside a reactor inside a specific rod should mimic the neutron flux distribution of the same fuel rod. Fig.3 shows the heat flux distribution for the “hot rod” of the TRIGA Mark II research reactor in AERE [31].

In order to obtain the temperature inside a fuel rod or cladding at a specific location at a given time, it is necessary to apply the three-dimensional unsteady-state energy equation with internal heat generation, which is given by,

$$\frac{1}{r} \frac{\partial}{\partial r} \left(kr \frac{\partial T}{\partial r} \right) + \frac{1}{r^2} \frac{\partial}{\partial \theta} \left(k \frac{\partial T}{\partial \theta} \right) + \frac{\partial}{\partial z} \left(k \frac{\partial T}{\partial z} \right) + \dot{q}''' = \frac{\partial}{\partial t} (\rho C_p T) \quad (9)$$

Here T is the local temperature of the solid (fuel or cladding) and ρ and C_p are the density and specific heat capacity of the solid respectively. Also, k is the thermal conductivity (W/m.K) of the element considered. In case of cladding, there is no volumetric heat generation and thus the term will be omitted from equation (9).

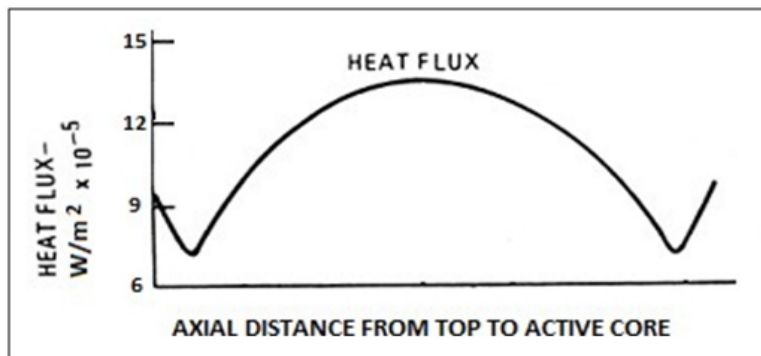


Fig. 3: Heat Flux Distribution Inside the “Hot Rod” in Axial Direction [31].

Fig.4 shows the typical construction of a fuel rod used in TRIGA Mark II research reactor in AERE. The dimension of each component of the fuel rod in two-dimensional coordinate system is shown in Fig.5. The fuel element is Uranium Zirconium Hydride ($U_{0.3}Zr_{1.6}H$), which has a much higher thermal conductivity compared to conventional nuclear fuel element i.e. Uranium Oxide (UO_2). The U-235 enrichment of fuel is also higher for research reactors, as stated earlier. It may be noted that the active length of the fuel element is 38.1 cm. There are graphite layers and stainless steel fittings on both end of the fuel rod, which have no active participation in the nuclear fission reaction. Graphite layers at the two sides act as reflectors.

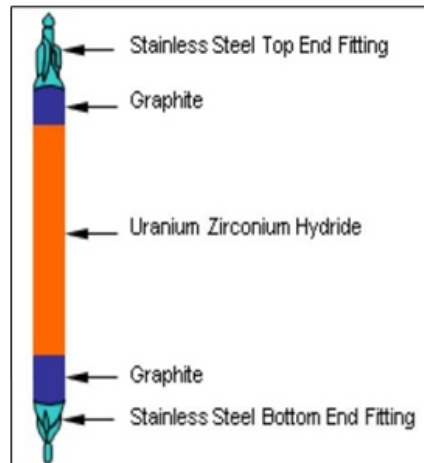


Fig. 4: Typical Construction of A TRIGA Mark II Reactor Fuel Rod [23].

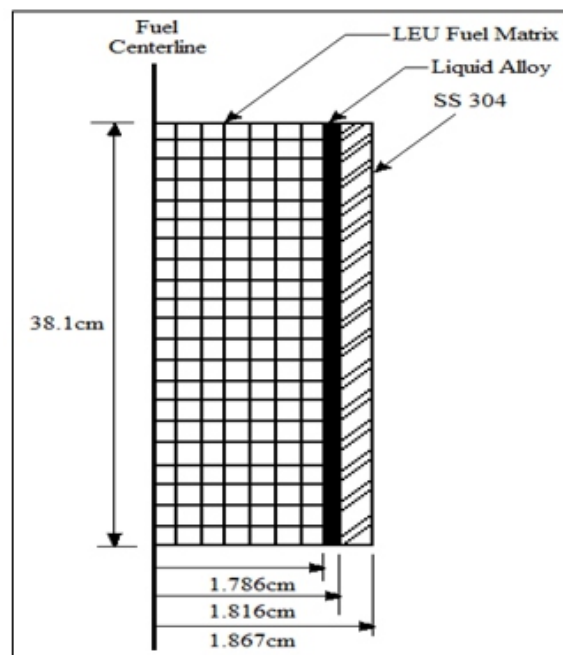


Fig. 5: Dimensions of Different Components of the Fuel Rod in 2-D Co-ordinate System.

The cladding material is made of SS 304 rather than Zircaloy. Another interesting variation in design of the fuel for TRIGA is that the gap between the fuel element and the cladding is filled up by a liquid alloy of Pb-Bi-Sn, which has a melting point lower than 100 °C. In case of conventional fuel rods in power

reactors, this gap is usually filled up by Helium gas. This modification in design has allowed the fuel centerline temperature to be maintained below 850 °C, which is necessary for avoiding fuel swelling and distortion [8]. Different compositions for the Pb-Bi-Sn liquid alloy are available. In this work, it has been assumed that the composition of the liquid alloy is 20% (Bi)-50% (Pb)-30% (Sn).

It may be noted that the gap between the fuel element and cladding is so small that the mode of heat transfer through the liquid alloy is mostly conduction. Therefore, equation (5) should hold for this region too. Of course, heat generation is absent in this region and thus should be omitted from equation (9).

The generated heat in the reactor core must be constantly removed to avoid heating of the fuel rods. TRIGA Mark II research reactor is a pool type reactor, the core being submerged in coolant water. This water, through either natural or forced convection, carries heat away from the system. Therefore, Newton's law of cooling is applicable for the coolant water, which is given by,

$$\dot{q}'' = h(T_{clad,out} - T_{\infty}) \quad (10)$$

Here, \dot{q}'' is heat flux (W/m^2), h is convection heat transfer coefficient ($W/m^2.K$), $T_{clad,out}$ is cladding outer surface temperature ($^{\circ}C$) and T_{∞} is bulk coolant temperature ($^{\circ}C$).

In order to determine convection heat transfer coefficient, it is necessary to determine the hydrodynamic parameters of the system. To do so, it is much more convenient to apply single channel flow analysis technique rather than performing analysis for the complex geometry of the reactor core structure.

2.3. Simulation techniques

An easy way to comply with the paper formatting requirements is to use this document as a template and simply type your text into it.

Before using Computational Fluid Dynamics (CFD) in analyzing the thermal-hydraulic behavior of a complex flow channel, it is necessary to simplify the geometry of the system. Single channel flow analysis is such a simplified method of analysis. In this method, it is assumed that there is a single flow channel around each fuel rod and each flow channel is unaffected by the adjacent flow channel. As a result, each fuel rod may be analyzed separately without worrying about the existence of the other fuel rods. This assumption reduces the difficulties in the analysis process and also reduces computation time. Fig.6b shows the single annular flow channel considered for this study. Also, a hot rod factor of 1.70 has been considered in this study in order to simulate the results for the fuel rod with highest amount of heat generation i.e. the “hot rod”.

The volumetric heat generation rate of reactor fuel element is not constant in the axial direction, as explained in the previous section. However, if it is assumed that there is variation in the axial direction, the CFD model becomes much simpler and should require less computation time. On the other hand, it may also affect the accuracy of the results obtained from simulation. Therefore, a comparative study has been conducted on the two possible methods of simulation; one in which it has been assumed that there is no variation of volumetric heat generation rate in the axial direction and the other one in which there is.

In this work, all the simulations have been conducted in COMSOL Multiphysics, a commercial simulation software that utilizes “Finite Element Method” (FEM). 2-D axis-symmetric model has been selected for conducting the simulation since the fuel rods are cylindrical. Utilizing a 2-D model instead of a 3-D model greatly reduces the computation time.

Fig.6 shows the simulation geometry in which there is no axial variation in heat generation. Since heat generation is uniform throughout the fuel element, it has been assumed that the fuel rod consists of a single, uniform fuel element.



Fig. 6: Simulation Geometry for No Axial Variation in Heat Generation.

Fig.7 shows the mesh distribution for the finite element analysis. Triangular mesh elements have been selected for as they are best suited for the physics behind conjugate heat transfer. From Fig.7, it may be noted that the mesh elements are finer near the outer boundary than the ones near the fuel centerline. The geometry consists of 32833 mesh elements with 3166 boundary elements.

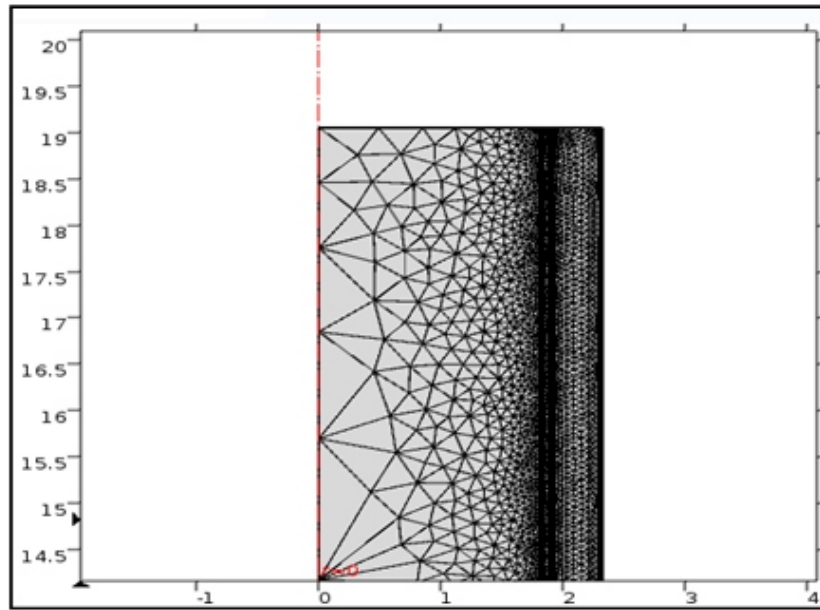


Fig. 7: Mesh Distribution of the Simulation Geometry for No Variation in Heat Generation.

Fig.8 shows the simulation geometry in which there is axial variation in heat generation. In order to accommodate axial variation effect in the simulation model, the fuel element has been divided in 13 regions along the axis. Each element has the same size with different volumetric heat generation rate. The variation in volumetric heat generation follows the pattern observed in Fig.3.

Fig.9 shows the mesh distribution for the finite element analysis of the model that accounts for axial variation in heat generation. From Fig.9, it may be observed that the mesh distribution is almost identical to that observed in Fig.7. A slight variation is observed due to the extra boundaries between the 13 separate regions of the fuel element. The mesh consists of 31469 mesh elements with 3306 boundary elements.

As the maximum coolant flow rate achievable is 13230 liters/min, the velocity of flow through the annular flow is calculated to be 0.207m/s. This flow velocity indicates turbulent flow. Therefore, $k-\omega$ turbulence model has been used for simulating the coolant-side thermal-hydraulic parameters. For simulating heat transfer through different regions of the fuel rod, it has been assumed that thermal conductivity, density and specific heat of each material remain constant for all temperatures. Table 1 presents the values of these parameters for different materials of concern.

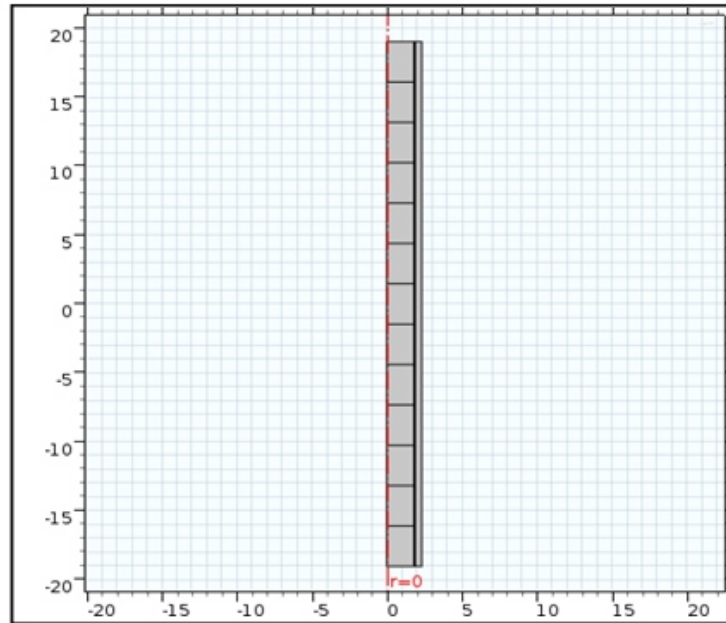


Fig. 8: Simulation Geometry for Axial Variation in Heat Generation.

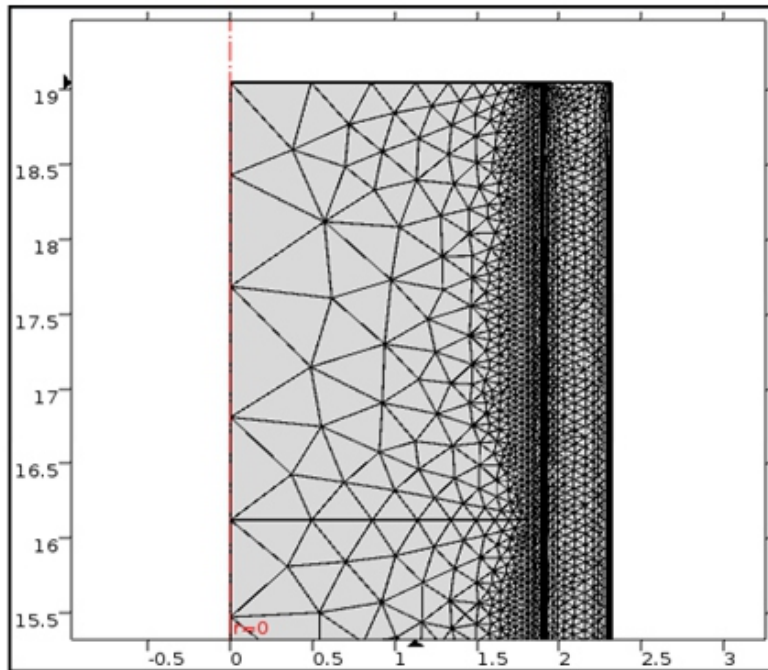


Fig. 9: Mesh Distribution of the Simulation Geometry for Axial Variation in Heat Generation.

Table 1: Properties of Different Materials

Material	k (W/m.K)	ρ (kg/m ³)	C _p (J/kg.K)
U0.3ZrH1.6	20 [8]	3715 [8]	-
SS 304	16.2 [32]	7800 [32]	507 [32]
Bi-Pb-Sn (20%-50%-30%)	38.9 [32]	9777 [32]	152.6 [32]

3. RESULTS AND DISCUSSION

In order to determine the performance of a simulation methodology in predicting a real-life scenario, the simulation results are compared with experimental data for validation. Fig.10 shows the typical pressure drop of the coolant while flowing through the reactor core in a TRIGA Mark II research reactor. From Fig.10, it may be observed that pressure drop is significant only at the entry and exit region of the coolant. There is no noticeable pressure drop while flowing past the fuel cladding surface. This may be due to the length of the fuel rod being so small (only 38.1 cm) that it doesn't cause a major pressure drop. Fig.11 and Fig.12 presents the calculated pressure values at various locations of the flow channel for both the simulation methods. From Fig.11 and Fig.12, it may be observed that the pressure drop across the flow channel due to friction is very small. From single fuel element simulation method, the pressure drop is calculated to be 2.248kPa. For multiple fuel pallet simulation method, pressure drop is found to be 2.261kPa. Both the values are insignificant, similar to the theoretical and real-life values. Therefore, it may be opined that both the simulation methods are capable of predicting pressure drop accurately. It is to be noted that the simulations are in 2-D and thus the losses due to entry and exit region are not considered.

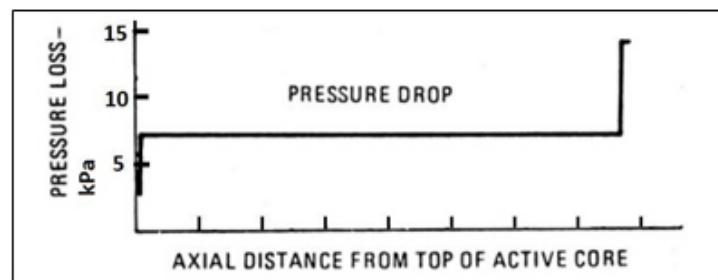


Fig. 10: Pressure Drop Along the Fuel Length for TRIGA Mark II Research Reactor [31].

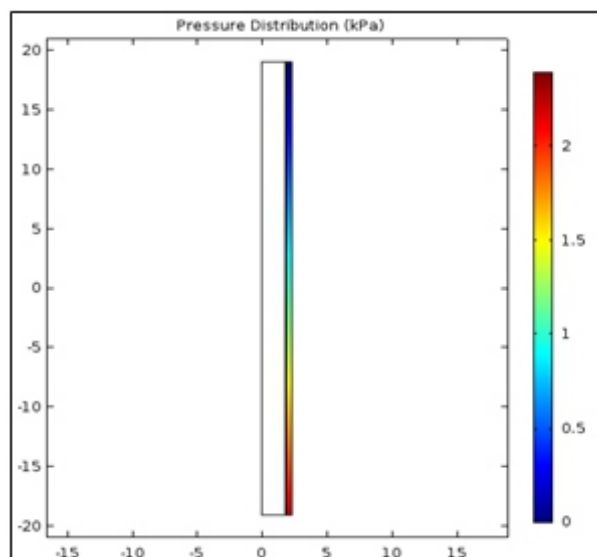


Fig. 11: Pressure Drop in Single Fuel Element Simulation Method.

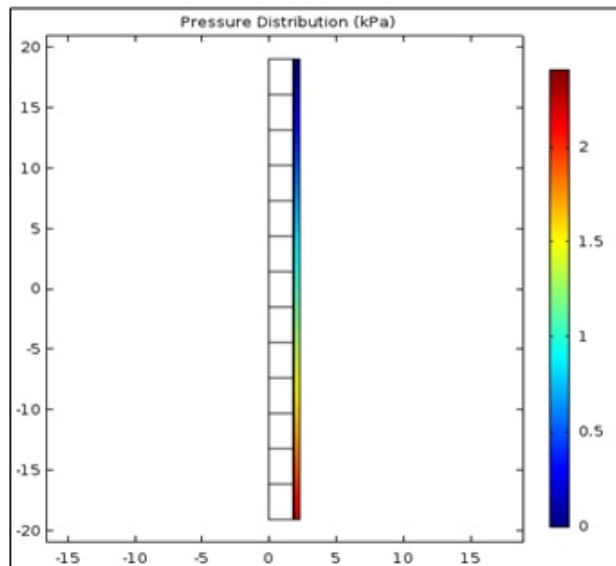


Fig. 12: Pressure Drop in Multiple Fuel Pallet Simulation Method.

Fig.13 shows the variation of temperature inside the fuel element if there is no variation in volumetric heat generation rate along the axis of the fuel. From Fig.13, it may be observed that there is almost no variation in temperature in the axial direction. However, variation in the radial direction is well-defined. The maximum temperature is observed to be along the centerline of the fuel element. The maximum temperature is above 700°C . Fig.14 shows the variation of temperature inside the fuel element if there is variation in volumetric heat generation rate along the axis of the fuel. From Fig.14, it may be observed that there is significant variation in temperature in both axial and radial direction. The maximum temperature is observed to be at the center of the fuel rod, both in axial and radial direction. Also, there is sufficient variation in the temperature distribution compared to that observed in Fig.14. The maximum temperature is just above 750°C .

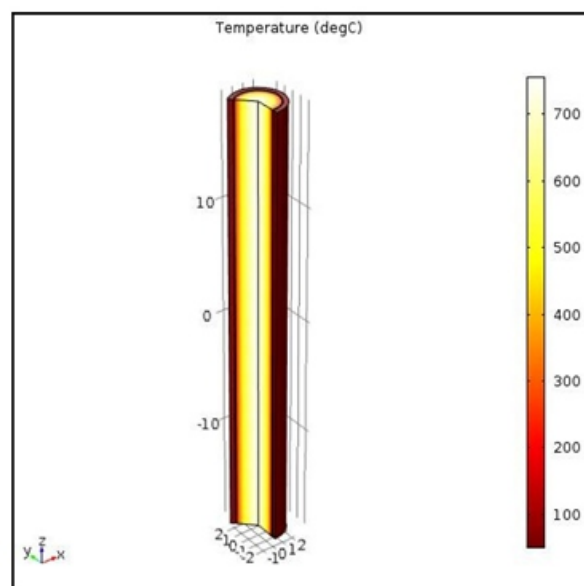


Fig. 13: Temperature Distribution Inside the Fuel Rod for No Axial Variation in Heat Generation Rate.

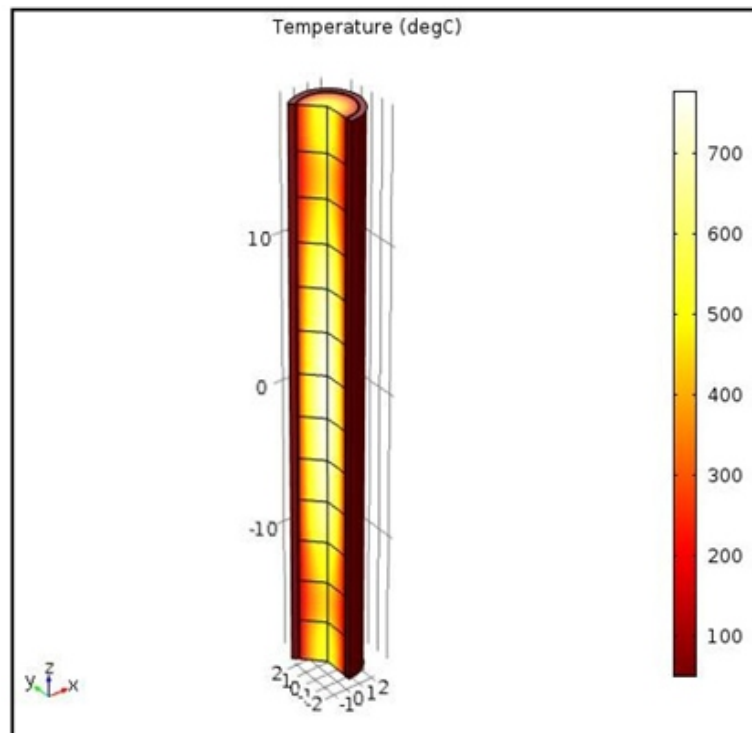


Fig. 14: Temperature Distribution Inside the Fuel Rod for Axial Variation in Heat Generation Rate.

Fig. 15 presents the variation of temperature along the axial distance at the fuel centerline obtained from experiments, theoretical calculations and both the simulation methods. From Fig. 15, it may be observed that the experimental data are quite different from the values predicted by the theoretical calculations. This is because theoretical calculations don't account for the reflector effects. For single fuel element simulation method, the maximum temperature of fuel centerline obtained is just above 750 oC, which is just a little lower than the experimental peak value. Also, the temperature is observed to be higher around the mid portion of the fuel rod compared to that at the end of the fuel rod. A similar trend is observed in the experimental data. However, the fuel centerline temperatures at the two ends are somewhat overestimated in the simulation results compared to the experimental data. This is because of the fact that volumetric heat generation has been constant throughout the fuel element, resulting in lesser variation in centerline temperature. On the other hand, there exists variation in heat generation along the axis of the fuel element in real condition and the rate of heat generation is much higher at the middle portion of the fuel rod compared to that at the ends. As a result, centerline temperature is measured to be higher in real-life condition than at the two ends. Since no variation has been accounted for in this simulation technique, the results have somewhat deviated from the actual condition. For multiple fuel pellet simulation method, the maximum temperature of fuel centerline is well above 750 oC, which is also very close to the experimental value. Also, the pattern of variation in temperature along axial distance is very similar to that observed in the experimental data. Finally, the fuel centerline

temperatures at the two ends are found to be almost the same as the experimental values. Since axial variation in volumetric heat generation rate has been accounted for in this simulation technique, the results have been very close to the actual values in almost any location along the centerline.

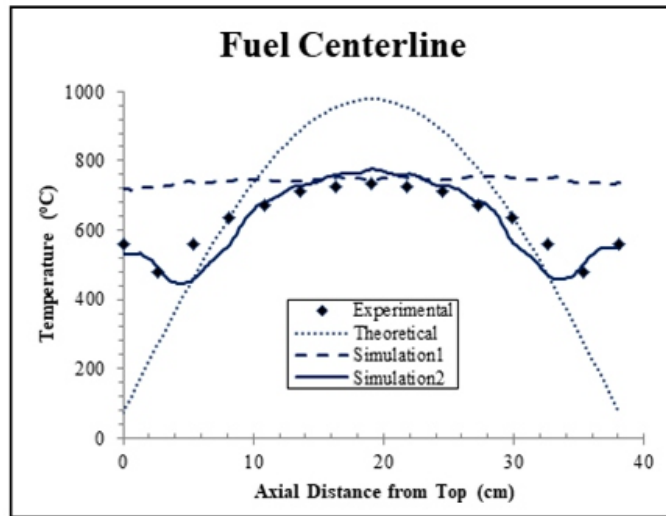


Fig. 15: Variation in Fuel Centerline Temperature for Different Tech-niques.

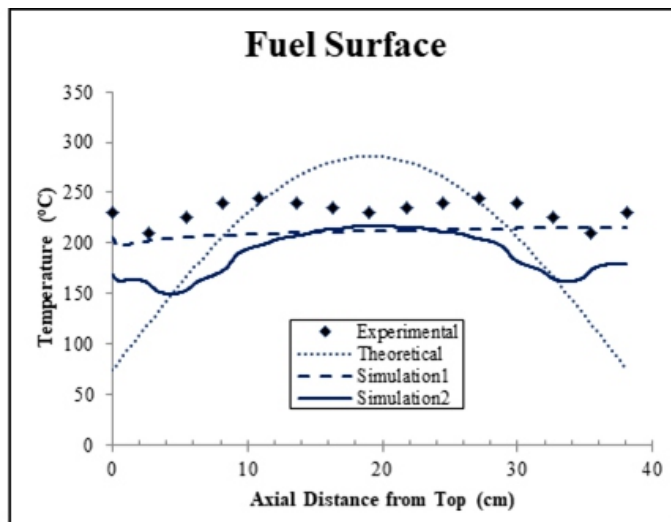


Fig. 16: Variation in Fuel Outer Surface Temperature for Different Tech- niques.

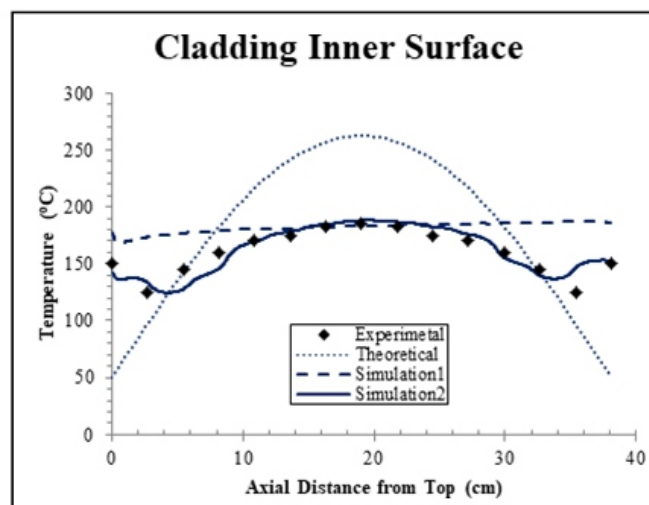


Fig. 17: Variation in Cladding Inner Surface Temperature for Different Techniques.

Fig.16 presents the variation of temperature along the axial distance at the fuel outer surface. From Fig.16, it may be observed that for single fuel element simulation method, fuel surface temperature is observed to be increasing along the length of the fuel rod. This is not the case in real situation. On the other hand, for multiple fuel pellet simulation method, it has been observed that the simulation results have varied a little the experimental data. In the experimental data, there is a decrease in temperature just at the middle portion of the fuel rod. In case of simulation results, however, the maximum temperature is observed to be at the middle portion, just the opposite of the experimental results. The possible reason behind this may be the assumption of constant thermal conductivity throughout the fuel element. In real case, however, there is variation in thermal conductivity of the fuel material with temperature. This issue may be resolved easily by using the actual relationship between thermal conductivity and temperature rather than using a constant value. Fig.17 presents the variation of temperature along the axial distance at the cladding inner surface. From Fig.17, it may be observed that for single fuel element simulation method, cladding inner surface temperature is observed to be increasing along the length of the fuel rod, just like fuel surface temperature. For multiple fuel pellet simulation method, the simulation results are almost identical to the experimental data.

It may be noted that there are small fluctuations in temperature distribution curves of both the simulation methods. These fluctuations have emerged because of taking finite number of steps (either 1 or 13 values) for volumetric heat generation rate instead of a continuous distribution. This fluctuation may be minimized by increasing the number of steps. However, this may increase computation time and difficulty.

From the above results, it may be stated that the simulation technique that adopts variation in volumetric heat generation rate along the axis of the fuel is sufficient to predict both the maximum temperature of the fuel and the temperature distribution inside the fuel rod with good accuracy. Therefore, this method is highly recommended for analysis. Nevertheless, both the simulation techniques yield better results compared to theoretical analysis.

4. CONCLUSION

In this work, the feasibility of employing “Single Flow Channel Analysis” technique alongside a CFD simulation tool for analyzing the thermal-hydraulic behavior of a TRIGA Mark II research reactor has been studied. COMSOL Multiphysics has been utilized as the thermal-hydraulic simulation tool. To identify the significance of accommodating axial variation of heat generation rate in the simulation model, two distinct geometries have been introduced. The first geometry consists of a single fuel element which has a volumetric heat generation rate equal to the average value of the same in the TRIGA

Mark II research reactor fuel. In the second geometry, the fuel element has been divided into 13 segments, similar to fuel pellets in real situation, each having different values of volumetric heat generation rate. As a result, the second geometry accounted for variation of heat generation in the axial direction. A hot rod factor of 1.70 has been taken for both cases in order to get simulation results for the “hot rod” of the reactor.

Since the fuel rods are arranged in hexagonal array inside the reactor core, the flow sub-channel should have a triangular cross-section. On the other hand, the flow sub-channel should be of annular cross-section for the simulation geometry. Therefore, necessary adjustments are made in the simulation geometry so that the hydraulic diameter remains the same. The flow velocity is taken 0.207m/s since the maximum flow rate is 13230 liters/min. This velocity should induce turbulence flow. Therefore, k- ω turbulence model has been selected for both simulations.

Results show that both the simulation techniques have superior performance compared to theoretical calculations. Again, for the simulation technique with no variation of heat generation rate in axial direction, there is almost no variation in temperature of the fuel centerline in the axial direction. However, the maximum temperature and its location for the fuel centerline are predicted with sufficient accuracy. The fuel centerline temperature has shown a maximum value just above 750 oC. The values of temperature on fuel centerline at other locations are predicted incorrectly. The simulation technique has also failed to resemble to actual characteristics curves of temperature at the fuel outer surface and cladding inner surface. On the other hand, the simulation technique in which there is variation in heat generation rate along the axis of the fuel, the results are highly similar to the experimental values. The curve representing the fuel centerline temperature is almost identical to the experimental curve. This technique has also predicted the temperature values at other locations inside the fuel rod that are in line with the experimental values.

This work has focused only on identifying the most suitable technique for analyzing the thermal behavior of the fuel rod in TRIGA reactor. This work may be extended to find the behavior of the fuel rod at different rates of heat generation and coolant flow rate. Also, the prospective use of other filler materials in the gap between the fuel and cladding may also be investigated. Finally, the optimum number of segments in the fuel element may be determined in order to obtain best results possible.

ACKNOWLEDGEMENT

The authors would like to thank Bangladesh Atomic Energy Commission (BAEC) for providing necessary experimental data for conducting this research. This work has not received any funding or grants from any individual or organization. The authors declare that there is no conflict of interests.

NOMENCLATURE

Symbol	Abbreviation
A	Area (m ²)
C _p	Heat Capacity (J/kg.K)
d	Diameter (m)
f	Friction Factor
g	Gravitational Constant (m/s ²)
H	Height (m)
k	Thermal Conductivity (W/m.K)
<i>m</i>	Mass Flow Rate (kg/s)
p	Pitch (m)
P	Pressure (Pa)
<i>q</i>	Linear Heat Generation Rate (W/m)
r	Radius (m)
T	Temperature (K)
ρ	Density (kg/m ³)

REFERENCES

- [1] Anglart H. *Applied Reactor Technology*. 2011.
- [2] Glaser A. *About the enrichment limit for research reactor conversion: Why 20%? In: International Meeting on Reduced Enrichment for Research and Test Reactors (hereinafter referred to as RERTR conference), Boston 2005 Nov 6.*
- [3] *TRIGA Power System: A Passive Safe Co-Generation Unit for Electric Power and Low Temperature Heat, Small Reactors for Low Temperature Heat Applications, IAEA-TECDOC-463 (International Atomic Energy Agency, Vienna, 1988) pp. 45-55.*
- [4] Yamanaka S, Yamada K, Kurosaki K, Uno M, Takeda K, Anada H, Matsuda T, Kobayashi S. *Thermal properties of zirconium hydride. Journal of Nuclear Materials*. 2001;294(1-2):94-8. [https://doi.org/10.1016/S0022-3115\(01\)00457-3](https://doi.org/10.1016/S0022-3115(01)00457-3).
- [5] Toma C, Parvan M, Tuturici IL. *Characterization of TRIGA LEU fuel behavior, irradiated in 14 MW core*. 2002.
- [6] Olander DR, Ng M. *Hydride fuel behavior in LWRs. Journal of nuclear materials*. 2005;346(2-3):98-108. <https://doi.org/10.1016/j.jnucmat.2005.05.017>.
- [7] Wongsawaeng D, Olander D. *Liquid-metal bond for LWR fuel rods. Nuclear Technology*. 2007;159(3):279-91. <https://doi.org/10.13182/NT07-A3876>.
- [8] Olander D, Greenspan E, Garkisch HD, Petrovic B. *Uranium–zirconium hydride fuel properties. Nuclear Engineering and Design*. 2009;239(8):1406-24. <https://doi.org/10.1016/j.nucengdes.2009.04.001>.
- [9] Žerovnik G, Snoj L, Trkov A, Barbot L, Fourmentel D, Villard JF. *Measurements of thermal power at the TRIGA Mark II reactor in Ljubljana using multiple detectors. IEEE Transactions on Nuclear Science*. 2014;61(5):2527-31. <https://doi.org/10.1109/TNS.2014.2356014>.
- [10] Nacir B, Boulaich Y, Chakir E, El Bardouni T, El Bakkari B, El Younoussi C. *Safety analysis and optimization of the core fuel re-loading for the Moroccan TRIGA Mark-II reactor. Annals of Nuclear Energy*. 2014;70:312-6. <https://doi.org/10.1016/j.anucene.2013.11.040>.
- [11] Agbo SA, Ahmed YA, Ewa IO, Jibrin Y. *Analysis of Nigeria re-search reactor-1 thermal power calibration methods. Nuclear Engineering and Technology*. 2016;48(3):673-83. <https://doi.org/10.1016/j.net.2016.01.014>.
- [12] Štancar Ž, Snoj L. *An improved thermal power calibration method at the TRIGA Mark II research reactor. Nuclear Engineering and Design*. 2017; 325:78-89. <https://doi.org/10.1016/j.nucengdes.2017.10.007>.
- [13] Cammi A, Ponciroli R, di Tigliole AB, Magrotti G, Prata M, Chiesa D, Previtali E. *A zero-dimensional model for simulation of TRIGA Mark II dynamic response. Progress in Nuclear Energy*. 2013; 68:43-54. <https://doi.org/10.1016/j.pnucene.2013.04.002>.
- [14] El Bakkari B, El Bardouni T, Nacir B, El Younoussi C, Boulaich Y, Boukhal H, Zoubair M. *Fuel burnup analysis for the Moroccan TRIGA research reactor. Annals of Nuclear Energy*. 2013; 51:112-9. <https://doi.org/10.1016/j.anucene.2012.07.030>.
- [15] Türkmen M, Çolak Ü. *Analysis of ITU TRIGA Mark II research reactor using Monte Carlo method. Progress in Nuclear Energy*. 2014; 77:152-9. <https://doi.org/10.1016/j.pnucene.2014.06.015>.

- [16] Coban R. Power level control of the TRIGA Mark-II research reactor using the multifeedback layer neural network and the particle swarm optimization. *Annals of Nuclear Energy*. 2014; 69:260-6. <https://doi.org/10.1016/j.anucene.2014.02.019>.
- [17] Alloni D, di Tigliole AB, Cammi A, Chiesa D, Clemenza M, Magrotti G, Pattavina L, Pozzi S, Prata M, Previtali E, Salvini A. Final characterization of the first critical configuration for the TRIGA Mark II reactor of the University of Pavia using the Monte Carlo code MCNP. *Progress in Nuclear Energy*. 2014; 74:129-35. <https://doi.org/10.1016/j.pnucene.2014.02.022>.
- [18] Henry R, Tiselj I, Snoj L. Analysis of JSI TRIGA MARK II reactor physical parameters calculated with TRIPOLI and MCNP. *Applied radiation and isotopes*. 2015; 97:140-8. <https://doi.org/10.1016/j.apradiso.2014.12.017>.
- [19] Mghar M, Chetaine A, Darif A. Calculation of kinetic parameters of the Moroccan TRIGA Mark-II reactor using the Monte Carlo code MCNP. *Advances in Applied Physics*. 2015;3(1):1-8. <https://doi.org/10.12988/aap.2015.531>.
- [20] Cammi A, Zanetti M, Chiesa D, Clemenza M, Pozzi S, Previtali E, Sisti M, Magrotti G, Prata M, Salvini A. Characterization of the TRIGA Mark II reactor full-power steady state. *Nuclear Engineering and Design*. 2016; 300:308-21. <https://doi.org/10.1016/j.nucengdes.2016.01.026>.
- [21] Čalić D, Žerovnik G, Trkov A, Snoj L. Validation of the Serpent 2 code on TRIGA Mark II benchmark experiments. *Applied Radiation and Isotopes*. 2016; 107:165-70. <https://doi.org/10.1016/j.apradiso.2015.10.022>.
- [22] Henry R, Tiselj I, Snoj L. CFD/Monte-Carlo neutron transport coupling scheme, application to TRIGA reactor. *Annals of Nuclear Energy*. 2017; 110:36-47. <https://doi.org/10.1016/j.anucene.2017.06.018>.
- [23] Manual for Description of the BAEC TRIGA Research Reactor. Bangladesh Atomic Energy Commission, 2012.
- [24] Lyric ZI, Mahmood MS, Motalab MA, Khan JH. Optimum burnup of BAEC TRIGA research reactor. *Annals of Nuclear Energy*. 2013; 55:225-9. <https://doi.org/10.1016/j.anucene.2012.12.019>.
- [25] Khan MJ, Sarker MM, Islam SM. Analysis of kinetic parameters of 3 MW TRIGA Mark-II research reactor using the SRAC2006 code system. *Annals of Nuclear Energy*. 2013; 60:181-6. <https://doi.org/10.1016/j.anucene.2013.05.009>.
- [26] Salam MA, Soner MA, Sarder MA, Haque A, Uddin MM, Sarker MM, Islam SM. Measurement of control rod reactivity and shut down margin of 3 MW TRIGA Mark-II research reactor using analogue and digital I&C system. *Annals of Nuclear Energy*. 2014; 68:257-61. <https://doi.org/10.1016/j.anucene.2014.01.030>.
- [27] Rahman MM, Akond MA, Basher MK, Huda MQ. Steady-state thermal-hydraulic analysis of TRIGA research reactor. *World Journal of Nuclear Science and Technology*. 2014;4(02):81. <https://doi.org/10.4236/wjnst.2014.42013>.
- [28] Salam MA, Soner MA, Sarder MA, Haque A, Uddin MM, Rahman A, Rahman MM, Sarkar MM, Islam SM. Measurement of neutronic safety parameters of the 3 MW TRIGA Mark-II research reactor. *Progress in Nuclear Energy*. 2014; 74:160-5. <https://doi.org/10.1016/j.pnucene.2014.02.025>.
- [29] Hosan MI, Soner MA, Kabir KA, Salam MA, Huq MF. Study on neutronic safety parameters of BAEC TRIGA research reactor. *Annals of Nuclear Energy*. 2015; 80:447-50. <https://doi.org/10.1016/j.anucene.2015.02.031>.
- [30] Hoq MA, Soner MM, Rahman A, Salam MA, Islam SM. Estimation of ^{41}Ar activity concentration and release rate from the TRIGA Mark-II research reactor. *Journal of environmental radioactivity*. 2016; 153:68-72. <https://doi.org/10.1016/j.jenvrad.2015.12.005>.
- [31] 3MW TRIGA-Mark-II Research Reactor's Safety Analysis Report, Bangladesh Atomic Energy Commission, 1986, General Atomics, USA.
- [32] Thermal properties of metals, metallic elements and alloys. Available online: https://www.engineeringtoolbox.com/thermal-conductivity-metals-d_858.html.

Empirical Models for Predicting Global Solar Radiation using Meteorological Parameters for Sokoto, Nigeria

Davidson O. Akpootu^{1*}, Bello I. Tijjani², Usman M. Gana²

¹Department of Physics, Usmanu Danfodiyo University, Sokoto, Nigeria

²Department of Physics, Bayero University, Kano, Nigeria

*Corresponding author_E-mail:davidson.odafe@udusok.edu.ng

ABSTRACT

The performances of sunshine, temperature and multivariate models for the estimation of global solar radiation for Sokoto (Latitude 13.020N, Longitude 05.250E and 350.8 m asl) located in the Sahelian region in Nigeria were evaluated using measured monthly average daily global solar radiation, maximum and minimum temperatures, sunshine hours, rainfall, wind speed, cloud cover and relative humidity meteorological data during the period of thirty one years (1980-2010). The comparison assessment of the models was carried out using statistical indices of coefficient of determination (R²), Mean Bias Error (MBE), Root Mean Square Error (RMSE), Mean Percentage Error (MPE), t – test, Nash – Sutcliffe Equation (NSE) and Index of Agreement (IA). For the sunshine based models, a total of ten (10) models were developed, nine (9) existing and one author's sunshine based model. For the temperature based models, a total of four (4) models were developed, three (3) existing and one author's temperature based model. The results of the existing and newly developed author's sunshine and temperature based models were compared and the best empirical model was identified and recommended. The results indicated that the author's quadratic sunshine based model involving the latitude and the exponent temperature based models are found more suitable for global solar radiation estimation in Sokoto. The evaluated existing Ångström type sunshine based model for the location was compared with those available in literature from other studies and was found more suitable for estimating global solar radiation. Comparing the most suitable sunshine and temperature based models revealed that the temperature based models is more appropriate in the location. The developed multivariate regression models are found suitable as evaluation depends on the available combination of the meteorological parameters based on two to six variable correlations. The recommended models are found suitable for estimating global solar radiation in Sokoto and regions with similar climatic information with higher accuracy and climatic variability.

Keywords: *Global Solar Radiation; Multivariate Models; Sokoto; Sunshine Based Model; Temperature Based Models.*

1. INTRODUCTION

Solar radiation is the energy transferred from the sun in the form of radiant to the earth's surface or it is simply the electromagnetic radiation emitted from the Sun. The most important parameter used in the design and evaluation of solar energy devices is the solar radiation. The sun through the emission of solar radiation provides about 99.97% of the heat energy required for physical processes [1]. The importance of solar radiation goes beyond its uses in everyday life; it is the primary source which allows existence of life on Earth. Along with its important role for existence, many human and environmental processes rely on the Sun's energy for natural development. Examples of these processes include the

evaporation of water which leads to precipitation, the photochemical processes involved with crop growth and the control of climatological conditions on Earth [2–3].

The traditional way to ascertain the amount of global solar radiation (GSR) in a particular region is to install pyranometers at as many locations as possible in this region thus requiring daily maintenance and data recording, and consequently increasing cost of GSR data collection. Thus, it is rather more economical to develop methods to estimate the GSR using climatological parameters [4]. Technical know-how for measuring solar radiation is costly and has instrumental hazards [5]. Therefore, alternative methods for estimating these data are required. One of these methods is the use of empirical models. Accurate modeling depends on the quality and quantity of the measured data used, and is a good tool for generating solar radiation at locations where measured data are not available [6].

Evidently, the best and most reliable information on solar radiation is that obtained from experimental measurements of the global and diffuse components of the solar insolation at the location in question. Regrettably, there are few meteorological stations conducting such measurements in developing countries such as Nigeria, this could be attributed to (i) inability to afford the measuring equipment due to the cost and (ii) lack of trained personnel to handle the measurement. Therefore, it is rather important to develop models to estimate the solar radiation using the available weather parameters.

Several models have been proposed to estimate global solar radiation. Ångström [7] was the first scientist known to suggest a simple linear relationship to estimate global solar radiation. Page [8] presents a linear regression model used in correlating the global solar radiation data with relative sunshine duration, which is a modified Ångström type model. Tijjani [9] determined a set of constants for Ångström – type correlation of the first and second order to estimate the monthly average daily global solar radiation for Katsina using five years (2005 – 2009) data of measured monthly global solar radiation and sunshine hours obtained from the Meteorological Department of the Federal Airport Authority of Nigeria (FAAN). According to him, the second order performed better than the first order based on the coefficient of correlation with 0.702 and 0.345 respectively. Muhammad and Darma [10] employed the monthly mean minimum/maximum temperature and relative humidity data obtained from Nigerian Meteorological Agency (NIMET), Abuja-Nigeria during the period of 6 years (2005 – 2010) to estimate the monthly average daily global solar radiation on a horizontal surface for Kano, Nigeria using modified Ångström models from which models were developed with regression coefficients a and b of $(1.2577 - 1.0167)$ and $(0.8317 - 0.0043)$ based on temperature ratio and relative humidity.

Olatona and Adeleke [11] developed some simple empirical models for the prediction of monthly mean daily solar radiation on a horizontal surface for Ibadan from sunshine hours and minimum and maximum temperatures data obtained from International Institute of Tropical Agriculture (IITA) Meteorological station at Ibadan, the data obtained covered a period of twenty years (1992 – 2011). Their results showed that the sunshine hour has lower mean errors than those based on minimum and maximum temperature which consistently produced an overestimation. Abdu and Abdullateef [12] used monthly mean data of sunshine hours obtained from the Nigerian Meteorological Agency (NIMET), Oshodi-Lagos, Nigeria during the period of 6 years (2009 – 2014) to estimate the global solar radiation for Zaria based on Angstrom – Prescott type model. The Ångström coefficients “a” and “b” obtained in their study are 0.3325 and 0.4510. The MBE and RMSE were also evaluated. Argungu and Dabai [13] compared linear and multivariate regression models for the estimation of global solar radiation in Sokoto, Nigeria using meteorological data of sunshine hours, relative humidity, minimum and maximum temperatures for a period of six years (2007 – 2012) obtained from the Nigerian Meteorological Agency (NIMET), Oshodi-Lagos, Nigeria. According to them, the best result was achieved using the model that combined sunshine hours, temperatures and natural logarithms of relative humidity. Girma [14] compare several existing sunshine and temperature based models using data on sunshine hours, minimum and maximum temperatures obtained from the Ethiopian Institute of Agricultural Research: Tepi National Spices Research Centre to estimate the global solar radiation for Tepi located in South West of Ethiopia. The monthly averages sunshine hour for 4 years (2013 – 2016) and monthly averages maximum and minimum temperatures for 5 years (2012 – 2016). The monthly averages daily global solar radiation from the Archives of National Aeronautics and Space Administration (NASA) for 22 years (July, 1983 – June, 2005) was utilized in his study. According to him, from the sunshine based models, the Samuel (polynomial) and the Newland (logarithm) models are appropriate for Tepi while the Chen et al model from the temperature based models is more appropriate for Tepi.

The purpose of this study is to develop new sunshine and temperature dependent models for estimating global solar radiation for Sokoto, Nigeria and to compare these developed models with existing models in literature to ascertain which of these models reliably estimate global solar radiation in the location under investigation. The evaluated existing Ångström type sunshine based model was also compared with those available in literature. Multivariate based models were also developed for the study area.

2. METHODOLOGY

2.1. Acquisition of data

It has been reported according to the World Meteorological Organization [15] and Ojo and Adeyemi [16] that to ensure the optimal climate modeling, data series should extend to at least thirty years long. In this regard, the measured monthly average daily global solar radiation, maximum and minimum temperatures, sunshine hours, rainfall, wind speed, cloud cover and relative humidity meteorological data during the period of thirty one years (1980-2010) was utilized in this study. The meteorological data were obtained from the Nigerian Meteorological Agency (NIMET), Oshodi, Lagos, Nigeria. Twenty five (25) years (1980 – 2004) data was used for developing the empirical models while six (6) years (2005 – 2010) data was used for the models validation.

2.2. Regression analysis

The first correlation proposed for estimating the monthly average global solar radiation is based on the method of Ångström [7]. The original Ångström- Prescott type regression equation relating monthly average daily radiation to clear day radiation in a given location and average fraction of possible sunshine hours is given by the equation:

$$\frac{H}{H_o} = a_1 + b_1 \left(\frac{S}{S_o} \right) \quad (1)$$

where H is the monthly average daily global solar radiation on a horizontal surface (MJ/m²/day), H_o is the monthly average daily extra-terrestrial radiation on a horizontal surface (MJ/m²/day), S is the monthly average daily hours of bright sunshine, S_o is the monthly average day length and a₁ and b₁ values are the Ångström empirical constants. The monthly average daily extraterrestrial radiation on a horizontal surface (H_o) can be calculated for days giving average of each month from the following equation [17–18]:

$$H_o = \left(\frac{24}{\pi} \right) I_{sc} \left[1 + 0.033 \cos \left(\frac{360n}{365} \right) \right] \left[\cos \phi \cos \delta \sin \omega_s + \left(\frac{2\pi \omega_s}{360} \right) \sin \phi \sin \delta \right] \quad (2)$$

where I_{sc} is the solar constant (=1367 Wm⁻²), φ is the latitude of the site, δ is the solar declination and ω_s is the mean sunrise hour angle for the given month and n is the number of days of the year starting from 1st of January to 31st of December.

The solar declination, δ and the mean sunrise hour angle, ω_s can be calculated using the following equation [17–18]:

$$\delta = 23.45 \sin \left\{ 360 \left(\frac{284+n}{365} \right) \right\} \quad (3)$$

$$\omega_s = \cos^{-1}(-\tan \phi \tan \delta) \quad (4)$$

For a given month, the maximum possible sunshine duration (monthly average day length (S_o)) in hours can be computed [17–18] by

$$S_o = \frac{2}{15} \omega \quad (5)$$

The clearness index (K_T) is defined as the ratio of the observed/measured horizontal terrestrial solar radiation H , to the calculated/predicted/estimated horizontal extraterrestrial solar radiation H_o [19].

$$K_T = \frac{H}{H_o} \quad (6)$$

In this study, H_o and S_o was computed for each month using equations (2) and (5) respectively.

Table 1: Sunshine Based Regression Models Proposed in the Literature that was adopted in this Study

Model No.	Model Type	Regression equation	Source
1	Linear (Angstrom)	$H_o = a + b \left(\frac{S}{S_o}\right)$	[7] and [20]
2	Quadratic	$H_o = a + b \left(\frac{S}{S_o}\right) + c \left(\frac{S}{S_o}\right)^2$	[21]
3	Cubic	$H_o = a + b \left(\frac{S}{S_o}\right) + c \left(\frac{S}{S_o}\right)^2 + d \left(\frac{S}{S_o}\right)^3$	[22]
4	Linear Logarithmic	$H_o = a + b \left(\frac{S}{S_o}\right) + c \ln \left(\frac{S}{S_o}\right)$	[23]
5	Logarithmic	$H_o = a + b \ln \left(\frac{S}{S_o}\right)$	[24]
	Linear		
6	Exponential	$H_o = a + b \left(\frac{S}{S_o}\right) + c \exp \left(\frac{S}{S_o}\right)$	[25]
7	Exponential	$H_o = a + b \exp \left(\frac{S}{S_o}\right)$	[26]
8	Linear	$H_o = a + b \left(\frac{S}{S_{nh}}\right)$	[27]
9	Exponent	$H_o = a \left(\frac{S}{S_o}\right)^b$	[25]

Model 8 is a modification of the Angström-PreScott model through the use of the ratio of $\left(\frac{S}{S_{nh}}\right)$ instead of $\left(\frac{S}{S_o}\right)$ by Louche et al. [27] and $\left(\frac{S}{S_{nh}}\right)$ is given by the relation: $\frac{1}{S_{nh}} = \frac{0.8706}{S_o} + 0.0003$

The proposed sunshine based model by the authors in this study is shown on Table 2

Table 2: Sunshine Based Regression Model Proposed in this Study

Model No.	Model Type	Regression equation	Source
10	Quadratic, latitude related	$H_o = a + b \cos \varphi \left(\frac{S}{S_o}\right) + c \cos \varphi \left(\frac{S}{S_o}\right)^2$	Authors

Table 3: Temperature Based Regression Models Proposed in Literature that was adopted in this Study

Model No.	Model Type	Regression equation	Source
1	Logarithmic	$H_o = a_2 + b_2 \ln \Delta T$	[28]
2	Linear exponent	$H_o = a_3 + b_3 \Delta T^{v_3}$	[29]
3	Linear	$H_o = a_4 + b_4 \left(\frac{\Delta T}{S_o}\right)$	[30]

where H , H_0 and S_0 are as previously defined. ΔT is the difference between the monthly average daily maximum and minimum temperatures, i.e., $T_{\max} - T_{\min}$

The constants a_2 , a_3 , a_4 , b_2 , b_3 , and b_4 in Table 3 are empirical coefficients determined by regression techniques and are also known as the regression coefficients and the other terms are the correlated parameters. The models are the three widely used temperature based models and are appropriate for different climatic conditions.

The proposed temperature based model by the authors in this study is given in Table 4.

Table 4: Temperature Based Regression Model Proposed in this Study

Model No.	Model Type	Regression equation	Source
4	Exponent	$\frac{H \Delta T^b}{H_0} = \alpha [(\)] S_0$	Authors

The models in Table 2 and 4 are proposed for this study in form of mathematical equations that relate the clearness index as the dependent variable with sunshine hour and temperature as the independent variables, also, are the multivariate models for other parameters. The proposed sunshine and temperature based models are simply a modification of the Ogelma et al and Garcia existing models. The essence of modification is to find out if it improves the accuracy of the existing models through modification.

The accuracy or validation of the estimated values was statistically tested by computing the MBE, RMSE, MPE, t-test, NSE and the IA, similarly, R^2 was determined for each of the models. The expressions for the MBE, RMSE and MPE as stated according to El-Sebaili and Trabea [31] are given as follows.

$$MBE = \frac{1}{n} \sum_{i=1}^n (H_{i,cal} - H_{i,mea}) \quad (7)$$

$$RMSE = \left[\frac{1}{n} \sum_{i=1}^n (H_{i,cal} - H_{i,mea})^2 \right]^{\frac{1}{2}} \quad (8)$$

$$MPE = \frac{1}{n} \sum_{i=1}^n \frac{H_{i,mea} - H_{i,cal}}{H_{i,mea}} * 100 \quad (9)$$

The t-test defined by student [32] in one of the tests for mean values, the random variable t with n-1 degrees of freedom may be written as follows.

$$t = \left[\frac{(n-1)(MBE)^2}{(RMSE)^2 - (MBE)^2} \right]^{\frac{1}{2}} \quad (10)$$

$$t = \left[\frac{(n-1)(MBE)^2}{(RMSE)^2 - (MBE)^2} \right]^{\frac{1}{2}} \quad (10)$$

The Nash-Sutcliffe equation (NSE) is given by the expression

$$NSE = 1 - \frac{\sum_{i=1}^n (H_{i,cal} - \bar{H}_{i,mea})^2}{\sum_{i=1}^n (H_{i,mea} - \bar{H}_{i,mea})^2} \quad (11)$$

The Index of Agreement (IA) is given as

$$IA = 1 - \frac{\sum_{i=1}^n (H_{i,cal} - \bar{H}_{i,mea})^2}{\sum_{i=1}^n (|H_{i,cal} - \bar{H}_{i,mea}| + |H_{i,mea} - \bar{H}_{i,mea}|)^2} \quad (12)$$

From equations (7) – (12) $H_{i,mea}$, $H_{i,cal}$ and n are respectively the i^{th} measured and i^{th} calculated values of daily global solar radiation and the total number of observations, also $\bar{H}_{i,mea}$ is the mean measured global radiation.

Chen et al. [28] have recommended that a zero value for MBE is ideal and a low RMSE and MPE are desirable. The smaller the value of the MBE, MPE and RMSE the better is the model's performance, a positive MPE and MBE values provide the averages amount of over-estimation in the calculated values, while the negative values gives underestimation. The percentage error between -10% and $+10\%$ is considered acceptable [33]. The smaller the value of R^2 , NSE and IA are desirable. The MBE and the RMSE are in $MJm^{-2}day^{-1}$, while R^2 , MPE, NSE and IA are in percentage (%), the t – test is non dimensional.

Multiple linear regression equation for estimating the global solar radiation with the clearness index been the dependent variable and the six independent meteorological variables is given as

$$\frac{H}{H_0} = a + bx_1 + \alpha_2 + \alpha_3 + \alpha_4 + \alpha_5 + \alpha_6 \quad (13)$$

where $a \dots \dots g$ are the regression coefficients and $x_1 \dots \dots x_6$ are the correlated parameters. The number of ways of combining the meteorological variables was obtained using the equation

$$n_{C_r} = \frac{n!}{(n-r)!r!} \quad (14)$$

where n is the total number of meteorological variables under study and r is the number of meteorological variables to be combined. In this study, the best five from the two, three and four variable regression equations and the best three from the five variable regression equations based on coefficient of determination was selected for further statistical analysis.

3. RESULTS AND DISCUSSION

3.1. Sunshine based models for Sokoto

The evaluated regression equation for the existing sunshine based models for Sokoto based on Table 1 are

$$\frac{H}{H_0} = 0.0749 + 0.809 \frac{S}{S_0} \quad (15a)$$

$$\frac{H}{H_0} = -0.655 + 3.05 \frac{S}{S_0} - 1.71 \left(\frac{S}{S_0}\right)^2 \quad (15b)$$

$$\frac{H}{H_0} = 1.09 - 5.1 \frac{S}{S_0} + 10.9 \left(\frac{S}{S_0}\right)^2 - 6.5 \left(\frac{S}{S_0}\right)^3 \quad (15c)$$

$$\frac{H}{H_0} = 2.05 - 1.30 \frac{S}{S_0} + 1.38 \ln \left(\frac{S}{S_0}\right) \quad (15d)$$

$$\frac{H}{H_0} = 0.832 + 0.530 \ln \left(\frac{S}{S_0}\right) \quad (15e)$$

$$\frac{H}{H_0} = 1.26 + 4.27 \frac{S}{S_0} - 1.79 \exp \left(\frac{S}{S_0}\right) \quad (15f)$$

$$\frac{H}{H_0} = -0.199 + 0.416 \exp \left(\frac{S}{S_0}\right) \quad (15g)$$

$$\frac{H}{H_0} = 0.0741 + 0.927 \frac{S}{S_0} \quad (15h)$$

$$\frac{H}{H_0} = 0.882 \left(\frac{S}{S_0}\right)^{0.893} \quad (15i)$$

The evaluated regression equation for the authors proposed sunshine based model for Sokoto based on Table 2 is

$$\frac{H}{H_0} = -0.655 + 3.13 \cos \varphi \left(\frac{S}{S_0}\right) - 1.75 \cos \varphi \left(\frac{S}{S_0}\right)^2 \quad (15j)$$

Table 5: A) Validation of the Sunshine Based Models for Sokoto under Different Statistical Test

Models	R ²	MBE	RMSE	MPE	t	NSE	IA
Eqn.15a	83.6	0.0093	0.8645	-0.1954	0.0357	97.4425	99.3503
Eqn.15b	85.1	-0.0950	0.8346	0.3393	0.3801	97.6168	99.3864
Eqn.15c	85.2	-0.4647	0.9499	2.0761	1.8605	96.9127	99.1466
Eqn.15d	85.0	0.1103	0.8403	-0.6304	0.4393	97.5840	99.4010
Eqn.15e	84.5	0.0196	0.8439	-0.2272	0.0769	97.5633	99.3835
Eqn.15f	85.1	-0.0370	0.8302	0.0660	0.1481	97.6416	99.3993
Eqn.15g	82.8	-0.0335	0.8836	-0.0035	0.1257	97.6416	99.3151
Eqn.15h	83.6	0.0130	0.8652	-0.2125	0.0497	97.4384	99.3497
Eqn.15i	83.6	-0.0129	0.8619	-0.0863	0.0495	97.4583	99.3521
Author's Model	R ²	MBE	RMSE	MPE	t	NSE	IA
Eqn.15j	85.1	-0.0301	0.8303	0.0329	0.1202	97.641	99.3999

Table 5: B) Ranking of the Evaluated Sunshine Based Models for Sokoto as Per Statistical Test

Models	R ²	MBE	RMSE	MPE	t	NSE	IA	Total Rank
Eqn.15a	5	1	7	5	1	7	7	33
Eqn.15b	2	8	3	8	8	3	4	36
Eqn.15c	1	10	10	10	10	10	10	61
Eqn.15d	3	9	4	9	9	4	1	39
Eqn.15e	4	4	5	7	4	5	5	34
Eqn.15f	2	7	1	3	7	1	3	24
Eqn.15g	6	6	9	1	6	1	9	38
Eqn.15h	5	3	8	6	3	9	8	42
Eqn.15i	5	2	6	4	2	6	6	31
Author's Models	R ²	MBE	RMSE	MPE	t	NSE	IA	Total Rank
Eqn.15j	2	5	2	2	5	2	2	20

Table 5A) and 5B) gives the summary of the various statistical tests adopted and ranking of the sunshine based models for Sokoto. Based on the R² the model, equation 15c (existing model) has the highest value with 85.2% and is judged the best model, while the model, equation 15g (existing model) has the lowest value with 82.8 %. Based on the MBE, the model, equation 15a (existing model) has the lowest value with overestimation of 0.0093 MJm⁻²day⁻¹ in the estimated value and is judged the best model, while the model, equation 15c (existing model) has the highest value with underestimation of 0.4697 MJm⁻²day⁻¹ in the estimated value. Based on the RMSE the model, equation 15f (existing model) has the lowest value with 0.8302 MJm⁻²day⁻¹ and is judged the best model, while the model, equation 15c (existing model) has the highest value with 0.9499 MJm⁻²day⁻¹. Based on the MPE, despite the observed overestimation and underestimation exhibited by some of the existing and researcher's models they all fall within the acceptable range ($MPE \leq \pm 10\%$) with the model, equation 15g (existing model) having the lowest value with underestimation of 0.0035% in the estimated value and is judged the best model, while the model, equation 15c (existing model) has the highest value with overestimation of 2.0761% in the estimated value. The study site was statistically tested at the (1 - α) confidence levels of significance of 95% and 99%. For the critical t-value, i.e., at α level of significance and degree of freedom, the calculated t-value must be less than the critical value ($t_{critical} = 2.20, df = 11, p < 0.05$) for 95% and ($t_{critical} = 3.12, df = 11, p < 0.01$) for 99%. It was observed that the $t_{cal} < t_{critical}$ values for all the models under consideration. The t - test shows that all models are significant at 95% and 99% confidence levels. However, the model, equation 15a (existing model) has the lowest value with 0.0357 and is judged the best model, while the model, equation 15c (existing model) has the highest value with 1.8605. Based on the NSE the models, equation 15f (existing model) and equation 15g (existing model) has the highest value with 97.6416 % and are judged the best models while the model, equation 15c (existing model) has the lowest value with 96.9127 %. Based on the IA the model, equation 15d (existing model) has the highest value with 99.4010 % and is judged the best model, while the model equation 15c (existing model) has the lowest value with 99.1466 %.

The ranking of the existing and author's model {Table 5B} was done based on the validation of the models {Table 5A}. The total ranks acquired by the different models were in the range 20 to 61. Based on the overall results for the sunshine based models for Sokoto, the model, equation 15j (author's model) is reported as the best and therefore most suitable for estimating global solar radiation in this location as compared to other evaluated sunshine based models. The model, equation 15f (existing model) was ranked 2nd most suitable model.

The 1st order Ångström type model results obtained for Sokoto in this study were compared to that carried out by Abdullahi and Sharafa [34]. The model equation with its empirical constants is given in equation 15a while the empirical constants given by Abdullahi and Sharafa [34] are 0.4785 and 0.2465. In this study the MBE, RMSE, MPE, and R2 were found to be 0.0093 MJm⁻²day⁻¹, 0.8645 %, -0.1954 % and 83.6 % respectively while the MBE, RMSE and R2 given by Abdullahi and Sharafa (2017) are 0.2990 %, 1.4324 % and 63.0 %. In another study Argungu and Dabai [13] obtained empirical constants of 0.0988 and 0.7875 with MBE, RMSE, MPE and R2 as -0.037 MJm⁻²day⁻¹, 1.512 MJm⁻²day⁻¹, -0.593 % and 32.15 %. Thus, this is evident that the model in this study performs better than their model based on the statistical test result. However, the model, equation 15r (author's model) is reported as the best and therefore most suitable for estimating global solar radiation in this location as compared to other evaluated sunshine based models.

Fig. 1A shows the comparison between the measured and estimated global solar radiation for Sokoto based on sunshine models. It is obvious that the estimated models underestimated the measured global solar radiation in the months from January to May and overestimated the measured global solar radiation in the months of June, July and September. The figure revealed that the model (Equation 15c) underestimated the measured and other estimated models in the months from January to May, August and from October to December; the model (Equation 15d) overestimated the measured and other estimated models in the months of June, July, September and October. In general, it can be seen from the figure that a good correlation existed between the measured and the models (Equation 15f and 15j) as compared to other evaluated models.

3.2 Temperature based models for Sokoto

The evaluated regression equations for the existing temperature based models for Sokoto based on Table 3 are

$$\frac{H}{H_0} = -0.0764 + 0.271 \ln \Delta T \quad (16a)$$

$$\frac{H}{H_0} = 0.0454 + 0.159 \text{ Sqrt } \Delta T \quad (16b)$$

$$\frac{H}{H_0} = 0.351 + 0.241 \frac{\Delta T}{S_0} \quad (16c)$$

The evaluated regression equation for the authors proposed temperature based models for Sokoto based on Table 4 is

$$\frac{H}{H_0} = 0.595 \left[\left(\frac{\Delta T}{S_0} \right) \right]^{0.407} \quad (16d)$$

Table 6: A) Validation of the Temperature Based Models for Sokoto under Different Statistical Test

Models	R ²	MBE	RMSE	MPE	t	NSE	IA
Eqn.16a	87.6	0.0156	0.7402	-0.0155	0.0698	98.1252	99.5392
Eqn.16b	87.8	0.0916	0.743	-0.3831	0.4119	98.1112	99.5415
Eqn.16c	93.2	0.0266	0.5435	-0.1341	0.1623	98.9893	99.7491
Author's Model	R ²	MBE	RMSE	MPE	t	NSE	IA
Eqn.16d	93.8	-0.0069	0.5269	0.0452	0.0433	99.05	99.7634

Table 6: B) Ranking of the Evaluated Temperature Based Models for Sokoto as Per Statistical Test

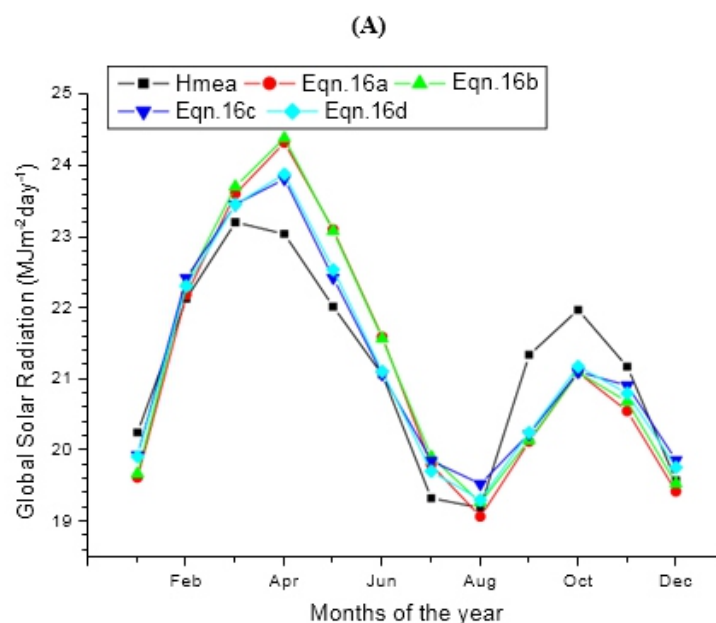
Models	R ²	MBE	RMSE	MPE	t	NSE	IA	Total Rank
Eqn.16a	4	2	3	1	2	3	4	19
Eqn.16b	3	4	4	4	4	4	3	26
Eqn.16c	2	3	2	3	3	2	2	17
Author's Models	R ²	MBE	RMSE	MPE	t	NSE	IA	Total Rank
Eqn.16d	1	1	1	2	1	1	1	8

Table 6A) and 6B) gives the summary of the various statistical tests adopted and ranking of the temperature based models for Sokoto. Based on the R² the model, equation 16d (author's model) has the highest value with 93.8 % and is judged the best model, while the model, equation 16a (existing model) has the lowest value with 87.6 %. Based on the MBE, the model, equation 16d (author's model) has the lowest value with underestimation of 0.0069 MJm⁻²day⁻¹ in the estimated value and is judged the best model, while the model, equation 16b (existing model) has the highest value with overestimation of 0.0916 MJm⁻²day⁻¹ in the estimated value. Based on the RMSE the model, equation 16d author's model) has the lowest value with 0.5269 MJm⁻²day⁻¹ and is judged the best model, while the model, equation 16b (existing model) has the highest value with 0.7430 MJm⁻²day⁻¹. Based on the MPE, despite the observed overestimation and underestimation exhibited by some of the existing and researcher's models they all fall within the acceptable range (MPE ±10%) with the model, equation 16a (existing model) having the lowest value with underestimation of 0.0155% in the estimated value and is judged the best model, while the model, equation 16b (existing model) has the highest value with underestimation of 0.3831 % in the estimated value. The study site was statistically tested at the (1 - α) confidence levels of significance of 95% and 99%. For the critical t-value, i.e., at α level of significance and degree of freedom, the calculated t-value must be less than the critical value (t_{critical} = 2.20, df = 11, < 0.05) for 95% and (t_{critical} = 3.12, df = 11, p < 0.01) for 99%. It was observed that t_{ca} < t_{critical} values for all the models under consideration. The t - test test shows that all models are significant at 95% and 99% confidence levels. However, the model, equation 16d (author's model) has the lowest value with 0.0433 and is judged the best model, while the model, equation 16b (existing model) has the highest value with 0.4119. Based on the NSE

the model, equation 16d (author's model) has the highest value with 99.0500 % and is judged the best models, while the model, equation 16b (existing model) has the lowest value with 98.1112 %. Based on the IA the model, equation 16d (author's model) has the highest value with 99.7634 % and is judged the best models, while the model, equation 16a (existing model) has the lowest value with 99.5392 %.

The ranking of the existing and author's models {Table 6B} was done based on the validation of the models {Table 6A}. The total ranks acquired by the different models were in the range 8 to 26. Based on the overall results for the temperature based models for Soko- to, the model, equation 16d (author's model) is reported as the best and therefore most suitable for estimating global solar radiation in this location as compared to other evaluated temperature based models. The model, equation 16c (existing model) was ranked 2nd most suitable model.

Fig. 1B shows the comparison between the measured and estimated global solar radiation for Sokoto based on temperature models. It is obvious that the estimated models underestimated the measured global solar radiation in the months of January, September, October and November and overestimated the measured global solar radiation in the months from February to July. The figure revealed that the model (Equation 16b) overestimated the measured and other estimated models in its estimated values in the months of March and April. Similarly, is the model (Equation 16c) in the months of February, August and December. The model (Equation 16a) underestimated the measured and other estimated models in the month of January, August, September, November and December. The figure depicts that all the evaluated models revealed a good correlation with the measured as there are no considerable deviation. However, it can be seen that a good correlation existed between the measured and the models (Equation 16c and 16d) as compared to other evaluated models.



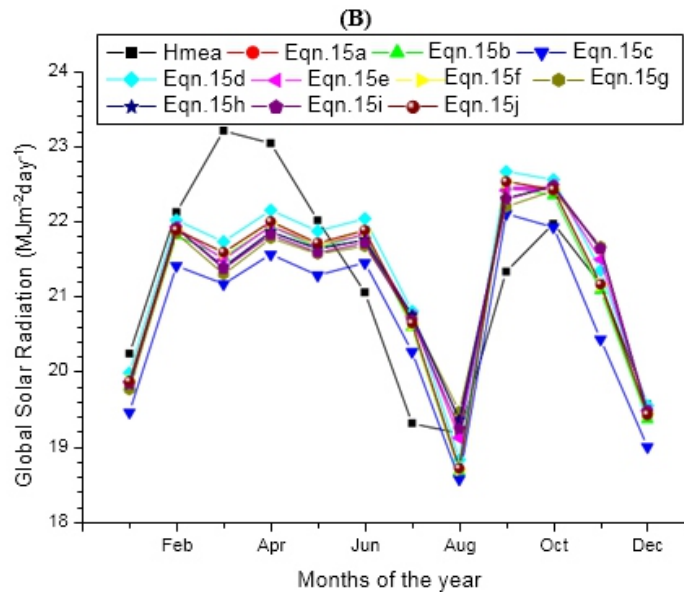


Fig. 1: Comparison between Measured and Estimated Global Solar Radiation for Sokoto (A) Sunshine Based Models (B) Temperature Based Models.

Table 7: Comparison/Ranking Between the Recommended Sunshine Based Models (SBM) and Temperature Based Models (TBM) for Sokoto

Sahelian	Models	Equation	R2	MBE	RMSE	MPE	t	NSE	IA	Total	Best
Sokoto	SBM	Eqn.15j	2	2	2	1	2	2	2	13	TBM
	TBM	Eqn.16d	1	1	1	2	1	1	1	8	

Table 7 shows that the temperature based model is more appropriate for estimating global solar radiation in the location under investigation. However, when temperature data are not available the sunshine hours data can reliably estimate global solar radiation using the proposed sunshine based model. According to Ajayi et al. [35], models with regard to Nigeria do not include the latitude, their accuracy and applications were limited to the sites from which the models were developed. Thus, the insertion of latitude in our sunshine based model makes it to some extent site independent and able to take into custody the differences due to variation in geographical locations. This is in line with that reported by Ajayi et al. [35]. The developed model is synonymous to the Ogelma et al model, except for the introduction of the cosine of locations latitude. For the temperature based model, the developed model is synonymous to Garcia model except that, it has power without a constant term. The model is site dependent and it's in line with the study reported by Huashan et al. [36] in China.

3.3. Multivariate regression models for Sokoto

The regression equations for two variable correlations for Sokoto are

$$H_0 = 0.364 + 0.411 \frac{S}{S_0} - 0.000492 RF \quad (17a)$$

$$\frac{H}{H_0} = 0.335 + 0.501 \frac{S}{S_0} - 0.00133 RH \quad (17b)$$

$$\frac{H}{H_0} = 0.816 - 0.00573 T_{mean} - 0.000793 RF \quad (17c)$$

$$\frac{H}{H_0} = 1.04 - 0.000656 RF - 0.0595 CC \quad (17d)$$

$$\frac{H}{H_0} = 0.695 - 0.00557 WS - 0.000825 RF \quad (17e)$$

where T_{mean} ($^{\circ}C$), is the mean temperature, S/S_0 is the sunshine duration, RF is the rainfall in mm, WS is the wind speed in ms^{-1} , CC is the cloud cover and RH is the relative humidity in (%).

Table 8: Validation of Multiple Linear Regression Models for Sokoto under Different Statistical Test for Two Variable Correlations

Models	R2	MBE	RMSE	MPE	t	NSE	IA
Eqn.17a	97.6	0.0117	0.3301	-0.0323	0.118	99.627	99.907
Eqn.17b	97.4	-0.0017	0.3397	-0.037	0.016	99.605	99.901
Eqn.17c	96.3	-0.0072	0.3671	0.0248	0.065	99.539	99.885
Eqn.17d	93.1	0.0645	0.5205	-0.2108	0.414	99.073	99.775
Eqn.17e	89.7	0.0238	0.667	-0.0025	0.119	98.478	99.629

Table 8 shows the summary of the various statistical tests performed on the two variable correlations for Sokoto, in order to ascertain the accuracies of the proposed models. Based on the R^2 , the model (Equation 17a) has the highest value and is judged as the best model. Based on the MBE it was observed that the models (Equation 17a, 17d and 17e) indicate overestimation in the estimated values, while the models Equation (17b and 17c) indicate underestimation in the estimated values. However, the model (Equation 17b) has the lowest MBE value as compared with all the developed models and was returned as the best performing model. Based on the RMSE, the model (Equation 17a) has the lowest value as compared to all the developed models and was returned as the best performing model. Based on the MPE, all the models exhibits underestimation in the estimated values, except the model (Equation 17c) that exhibit overestimation in the estimated values, all the evaluated models perform better as they are all within the acceptable range of -10% and $+10\%$ with the model (Equation 17e) having the lowest value and was judged the best. The study location was statistically tested at the $(1 - \alpha)$ confidence levels of significance of 95% and 99%. The t - test shows that all models are significant at 95% and 99% confidence levels with the model (Equation 17b) having the lowest value and was judged the best. Based on the NSE and IA the model (Equation 17a) has the highest value with 99.6272 % and 99.9074 % and is judged the best. It was observed that all the developed models are found suitable for predicting global solar radiation with higher accuracies.

Fig. 2A shows the comparison between the measured and the estimated global solar radiation for two variable correlations in Sokoto. It is obvious that the model (Equation 17e) underestimated the measured

and other estimated models in the months of January, February and July and overestimated in its estimated values in the months of March to May. The model (Equation 17d) overestimated and underestimated the measured and other models in the months of October and December respectively. The model (Equation 17a) shows overestimation in the months of June and September and underestimation in the month of August as compared to the measured and other estimated models. The figure shows that all the estimated models overestimated the measured in the month of June. In general, all the estimated models exhibit good correlation with the measured.

The regression equations for three variable correlations for Sokoto are

$$\frac{H}{H_0} = 0.374 + 0.423 \frac{S}{S_0} - 0.000278 RF - 0.000698 RH \quad (18a)$$

$$\frac{H}{H_0} = 0.437 + 0.455 \frac{S}{S_0} - 0.00771 WS - 0.00162 RH \quad (18b)$$

$$\frac{H}{H_0} = 0.535 + 0.285 \frac{S}{S_0} - 0.00288 T_{mean} - 0.000584 RF \quad (18c)$$

$$\frac{H}{H_0} = 1.04 - 0.00482 T_{mean} - 0.000705 RF - 0.0381 CC \quad (18d)$$

$$\frac{H}{H_0} = 0.509 + 0.364 \frac{S}{S_0} - 0.000487 RF - 0.0173 CC \quad (18e)$$

Table 9: Validation of Multiple Linear Regression Models for Sokoto under Different Statistical Test for Three Variable Correlations

Models	R2	MBE	RMSE	MPE	t	NSE	IA
Eqn.18a	98.8	-0.0095	0.2412	0.0483	0.1313	99.801	99.95
Eqn.18b	98.7	0.0108	0.24	-0.0813	0.15	99.803	99.951
Eqn.18c	98.7	0.0014	0.2349	-0.0156	0.0199	99.811	99.953
Eqn.18d	97.9	0.0587	0.2765	-0.2752	0.721	99.738	99.935
Eqn.18e	97.9	-0.0101	0.3053	0.0776	0.1096	99.681	99.921

Table 9 shows the summary of the various statistical tests performed on the three variable correlations for Sokoto, in order to ascertain the accuracies of the proposed models. Based on the R^2 , the model (Equation 18a) has the highest values and is judged as the best model. Based on the MBE it was observed that the models (Equation 18b, 18c and 18d) indicate overestimation in the estimated values, while the models (Equation 18a and 18e) indicate underestimation in the estimated values. However, the model (Equation 18c) has the lowest MBE value as compared with all the developed models and was returned as the best performing model. Based on the RMSE, the model (Equation 18c) has the lowest value as compared to all the developed models and was returned as the best performing model. Based on the MPE, the models (Equation 18b, 18c and 18d) exhibits underestimation in the estimated values while the models (Equation 18a and 18e) exhibit overestimation in the estimated values, all the evaluated models perform better as they are all within the acceptable range of -10% and $+10\%$ with the model

(Equation 18c) having the lowest value and was judged the best. The study location was statistically tested at the $(1 - \alpha)$ confidence levels of significance of 95% and 99%. The t - test shows that all models are significant at 95% and 99% confidence levels with the model (Equation 18c) having the lowest value and was judged the best. Based on the NSE and IA the model (Equation 18c) has the highest value with 99.8112 % and 99.9528 % and is judged the best model. The developed models are found suitable for predicting global solar radiation with higher accuracies.

Fig. 2B shows the comparison between the measured and the estimated global solar radiation for three variable correlations in Sokoto. It is obvious that the model (Equation 18d) overestimated the measured and other estimated models in the months of January, April and August and underestimated in its estimated values in the months of July and November. The model (Equation 18e) overestimated in the months of May, June, September and October and underestimated the measured and other models in the months of January August and December respectively. The figure shows that all the estimated models overestimated the measured in the month of April also in the month of May and June except for the model (Equation 18b). In general, all the estimated models exhibit good correlation with the measured.

The regression equations for four variable correlations for Sokoto are

$$\frac{H}{H_0} = 0.453 + 0.397 \frac{S}{S_0} - 0.00648 WS - 0.000234 RF - 0.00104 RH \quad (19a)$$

$$\frac{H}{H_0} = 0.711 + 0.225 \frac{S}{S_0} - 0.00300 T_{mean} - 0.000582 RF - 0.0201 CC \quad (19b)$$

$$\frac{H}{H_0} = 0.474 + 0.343 \frac{S}{S_0} - 0.00173 T_{mean} - 0.000409 RF - 0.000453 RH \quad (19c)$$

$$\frac{H}{H_0} = 0.515 + 0.378 \frac{S}{S_0} - 0.000274 RF - 0.0168 CC - 0.000694 RH \quad (19d)$$

$$\frac{H}{H_0} = 0.382 + 0.485 \frac{S}{S_0} - 0.00766 WS + 0.00116 T_{mean} - 0.00158 RH \quad (19e)$$

Table 10: Validation of Multiple Linear Regression Models for Sokoto under Different Statistical Test for Four Variable Correlations

Models	R2	MBE	RMSE	MPE	t	NSE	IA
Eqn.19a	99.7	-0.0072	0.1244	0.0422	0.1936	99.9471	99.9868
Eqn.19b	99	-0.0133	0.1978	0.0604	0.2234	99.8661	99.9664
Eqn.19c	99	0.0159	0.2104	-0.0842	0.2518	99.8485	99.9622
Eqn.19d	99	-0.0048	0.211	0.0325	0.0756	99.8477	99.962
Eqn.19e	99	0.0253	0.2105	-0.1269	0.402	99.8484	99.9622

Table 10 shows the summary of the various statistical tests performed on the four variable correlations for Sokoto, in order to ascertain the accuracies of the proposed models. Based on the R^2 , the model (Equation 19a) has the highest values and is judged as the best model. Based on the MBE it was observed that the models (Equation 19a, 19b and 19d) indicate underestimation in the estimated values, while the

models (Equation 19c and 19e) indicate overestimation in the estimated values. However, the model (Equation 19d) has the lowest MBE value as compared with all the developed models and was returned as the best performing model. Based on the RMSE, the model (Equation 19a) has the lowest value as compared to all the developed models and was returned as the best performing model. Based on the MPE, the models (Equation 19c and 19e) exhibits underestimation in the estimated values while the models (Equation 19a, 19b and 19d) exhibit overestimation in the estimated values, all the evaluated models perform better as they are all within the acceptable range of -10% and $+10\%$ with the model (Equation 19d) having the lowest value and was judged the best. The study location was statistically tested at the $(1 - \alpha)$ confidence levels of significance of 95% and 99%. The t - test shows that all models are significant at 95% and 99% confidence levels with the model (Equation 19d) having the lowest value and was judged the best. Based on the NSE and IA the model (Equation 19a) has the highest value with 99.9471 % and 99.9868 % and is judged the best model. It was observed that all the developed models are found suitable for predicting global solar radiation with higher accuracies.

Fig. 2C shows the comparison between the measured and the estimated global solar radiation for four variable correlations in Sokoto. It is obvious that the model (Equation 19e) overestimated the measured and other estimated models in the months of February, March, July and November and underestimated in its estimated values in the months of January, May and June. The model (Equation 19b) overestimated in the months of January, September and October and underestimated the measured and other models in the months of July and November respectively. The figure shows that all the estimated models overestimated the measured in the month of April also except for the model (Equation 19b) in the month of July. In general, all the estimated models exhibit good correlation with the measured.

The regression equations for five variable correlations for Sokoto are

$$\frac{H}{H_0} = 0.515 + 0.345 \frac{S}{S_0} - 0.00605 WS + 0.00116 T_{\text{mean}} - 0.000325 RF - 0.000850 RH \quad (20a)$$

$$\frac{H}{H_0} = 0.484 + 0.387 \frac{S}{S_0} - 0.00614 WS - 0.000236 RF - 0.00420 CC - 0.00102 RH \quad (20b)$$

$$\frac{H}{H_0} = 0.643 + 0.283 \frac{S}{S_0} - 0.00193 T_{\text{mean}} - 0.000419 RF - 0.0188CC - 0.000420 RH \quad (20c)$$

Table 11: Validation of Multiple Linear Regression Models for Sokoto under Different Statistical Test for Five Variable Correlations

Models	R2	MBE	RMSE	MPE	t	NSE	IA
Eqn.20a	99.8	0.0187	0.1055	-0.0889	0.5957	99.9619	99.9905
Eqn.20b	99.7	-0.0123	0.1228	0.0676	0.333	99.9484	99.9871
Eqn.20c	99.3	0.0046	0.1705	-0.0252	0.0903	99.9005	99.9751

Table 11 shows the summary of the various statistical tests performed on the five variable correlations for Sokoto, in order to ascertain the accuracies of the proposed models. Based on the R^2 , the model

(Equation 20a) has the highest values and is judged as the best model. Based on the MBE it was observed that the models (Equation 20a and 20c) indicate overestimation in the estimated values, while the model (Equation 20b) indicates underestimation in the estimated values. However, the model (Equation 20c) has the lowest MBE value as compared with all the developed models and was returned as the best performing model. Based on the RMSE, the model (Equation 20a) has the lowest value as compared to all the developed models and was returned as the best performing model. Based on the MPE, all the models exhibits underestimation in the estimated values, except the model (Equation 20b) that exhibit overestimation in the estimated values, all the evaluated models perform better as they are all within the acceptable range of -10% and $+10\%$ with the model (Equation 20c) having the lowest value and was judged the best. The study location was statistically tested at the $(1 - \alpha)$ confidence levels of significance of 95% and 99%. The t - test shows that all models are significant at 95% and 99% confidence levels with the model (Equation 20c) having the lowest value and was judged the best while the model (Equation 20a) has the highest. Based on the NSE and IA the model (Equation 20a) has the highest value with 99.9619 % and 99.9905 % and is judged the best model. It was observed that all the developed models are found suitable for predicting global solar radiation with higher accuracies.

Fig. 2D shows the comparison between the measured and the estimated global solar radiation for five variable correlations in Sokoto. The figure shows that all the estimated models underestimated the measured in the months of March and August and overestimated the measured in the months of April and July. It is obvious that the model (Equation 20c) overestimated the measured and other estimated models in the months of January, February, May and June and underestimated in its estimated values in the months from August to December. The model (Equation 20a) overestimated the measured and other estimated models in the months of September and December. In general, all the estimated models exhibit good correlation with the measured.

The regression equations for six variable correlation for Sokoto is

$$\frac{H}{H_0} = 0.573 + 0.322 \frac{S}{S_0} - 0.00544 WS - 0.00130 T_{mean} - 0.000338 RF - 0.00697 CC - 0.000797 RH \quad (21)$$

Table 12: Validation of Multiple Linear Regression Models for Sokoto under Different Statistical Test for Six Variable Correlations

Models	R2	MBE	RMSE	MPE	t	NSE	IA
Eqn.21	99.8	-0.0259	0.101	0.1232	0.88	99.965	99.991

All the statistical test analysis for the six variable correlations shown on Table 12 shows high statistical significant relationship between the estimated and measured global solar radiation based on the six meteorological variables used in the study site. Therefore, could be used for predicting global solar radiation with higher accuracies as evaluation depends on the available combination of the six meteorological parameters based on the developed model.

Fig. 2E shows the comparison between the measured and the estimated global solar radiation for six variable correlation in Sokoto. The figure shows that there is no considerable deviation between the estimated model and the measured. Though, the estimated model under- estimated the measured in the months of January, March, May, June, August, October, November and December and overestimated the measured in the months of February, April, July and September. In general, the estimated model exhibit good correlation with the measured.

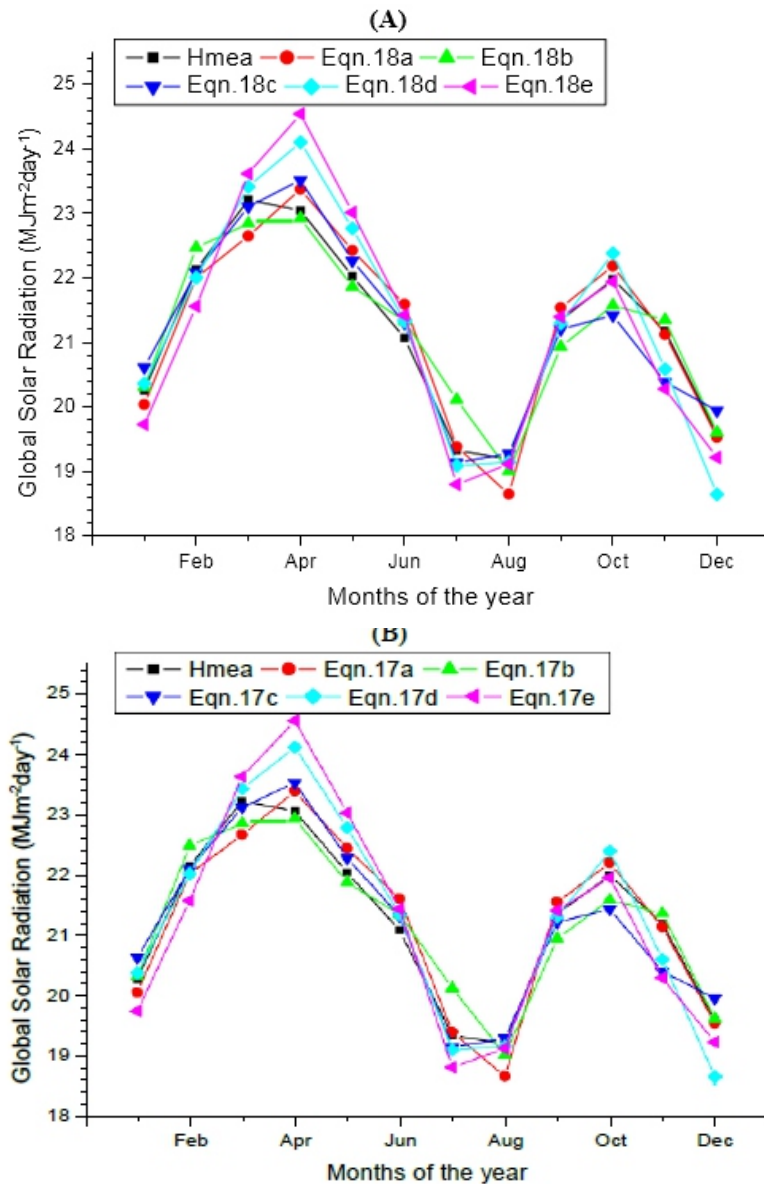


Fig. 2E shows the comparison between the measured and the estimated global solar radiation for six variable correlation in Sokoto. The figure shows that there is no considerable deviation between the estimated model and the measured. Though, the estimated model under- estimated the measured in the months of January, March, May, June, August, October, November and December and overestimated the measured in the months of February, April, July and September. In general, the estimated model exhibit good correlation with the measured.

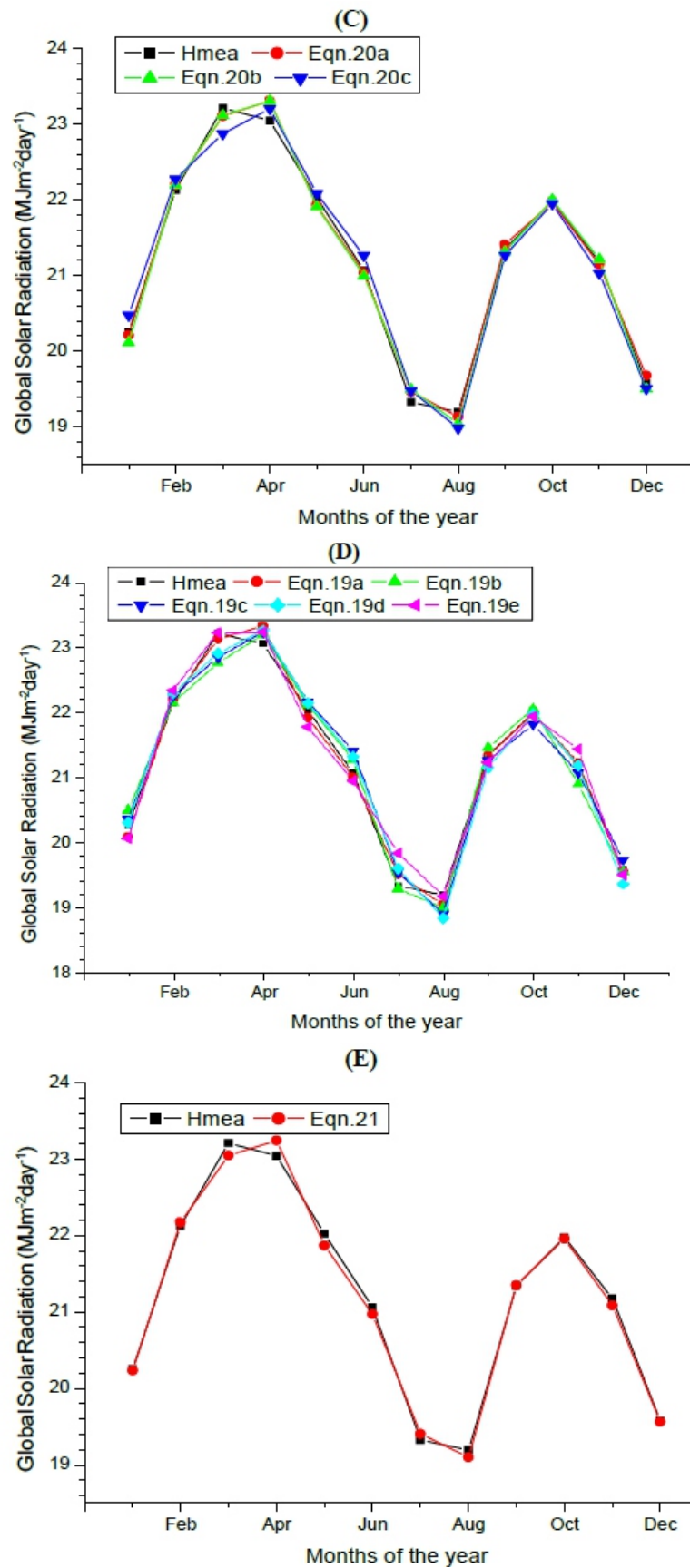


Fig. 2: Comparison between Measured and Estimated Global Solar Radiation for Sokoto (A) Two Variable Correlations (B) Three Variable Correlations (C) Four Variable Correlations (D) Five Variable Correlations (E) Six Variable Correlation.

4. CONCLUSION

A wide-ranging study was carried out to help in the selection of the most fitting and accurate models based on the statistical test indicators of coefficient of determination (R^2), Mean Bias Error (MBE), Root Mean Square Error (RMSE), Mean Percentage Error (MPE), t – test, Nash – Sutcliffe Equation (NSE) and Index of Agreement (IA) using meteorological parameters of measured monthly average daily global solar radiation, maximum and minimum temperatures, sunshine hours, rainfall, wind speed, cloud cover and relative humidity meteorological data during the period of thirty one years (1980-2010) for Sokoto located in the Sahelian region in Nigeria. The evaluated models are classified into three categories namely, sunshine, temperature and multivariate based. In each category, the most accurate models are identified and presented. A total of ten (10) sunshine based models were evaluated and compared out of which nine (9) are existing models and one newly developed author's model. A total of four (4) temperature based models were evaluated and compared, three (3) existing and one newly developed author's temperature based model. The results indicated that the modified author's newly developed sunshine and temperature based models produces more accurate global solar radiation estimates than the existing models examined for the studied location.

The evaluated existing Ångström type sunshine based model was found more suitable for estimating global solar radiation when compared to those available in literature from other studies. This may be attributed to the quality and quantities of the data used in this study as they met the World Meteorological Organization (WMO) standards. The correlation between the measured and evaluated models shows overestimation and underestimation in their evaluated values in some months with the temperature based models been more correlated. The new temperature based model was found more appropriate for global solar radiation in the location when compared to the new sunshine based model. In general, all the developed multivariate regression models are found appropriate as evaluation relies on the obtainable combination of the meteorological parameters based on two to six variable correlation and they all exhibited good correlation with the measured. It is believed that this study has addressed the issue of estimating global solar radiation with higher accuracy for Sokoto, Nigeria.

ACKNOWLEDGEMENT

The authors are grateful to the management and staff of the Nigerian Meteorological Agency (NIMET), Oshodi, Lagos for providing all the necessary data used in this present study. The anonymous reviewers are also appreciated.

FUNDING

This research did not receive any specific grant from funding agencies in the public, commercial, or not-for-profit sectors.

REFERENCES

- [1] E. O. Ogolo, *Evaluating the performance of some predictive models for estimating global solar radiation across varying climatic conditions in Nigeria*. *Indian Journal of Radio & space Physics*, 39 (2010) 121-131.
- [2] B. Viorel, *Modeling solar radiation at the earth's surface: Recent advances*. Springer. (2008)
- [3] M. S. Dresselhaus, I. L. Thomas, *Alternative Energy Technologies*. *Nature*, 414 6861 (2001) 332-337. <https://doi.org/10.1038/35104599>.
- [4] A. Kassem, A. Aboukarima, N. El Ashmawy, *Development of Neural Network Model to Estimate Hourly Total and Diffuse Solar Radiation on Horizontal Surface at Alexandria City (Egypt)*, *Journal of Applied Sciences Research*, 5, 11 (2009) 2006-2015.
- [5] M. Alam, S. Saha, M. Chowdhury, M. Rahman, *Simulation of Solar Radiation System*, *Am. J. Appl. Sci*, 2,4 (2005) 751 – 758. <https://doi.org/10.3844/ajassp.2005.751.758>.
- [6] A. Al-Salihi, M. Kadum, A. Mohammed, *Estimation of Global Solar Radiation on Horizontal Surface Using Meteorological Measurement for different Cities in Iraq*, *Asian J. Sci. Res*, 3, 4 (2010) 240 – 248. <https://doi.org/10.3923/ajsr.2010.240.248>.
- [7] A. Ångström, *Solar and terrestrial radiation*. *Quarterly Journal of the Royal Meteorological society*, 50 (1924) 121-125.
- [8] J. K. Page, *The estimation of monthly mean values of daily total short – wave radiation on vertical and inclined surfaces from sunshine records for latitude 40° N - 40° S*. *Proceeding of the UN Conference on New Sources of Energy, Rome*, 4 (1964) 378 – 390.
- [9] B. I. Tijjani, *Comparison between first and second order Ångström type models for sunshine hours at Katisna, Nigeria*. *Bayero Journal of Pure and Applied Sciences*, 4 (2011) 24-27. <https://doi.org/10.4314/bajopas.v4i2.5>.
- [10] A. Muhammad, T. H. Darma, *Estimation of Global Solar Radiation for Kano State Nigeria Based on Meteorological Data*, *IOSR Journal of Applied Physics*, 6, 1 (2014) 19 – 23. <https://doi.org/10.9790/4861-06611923>.
- [11] G. I. Olatona, A. E. Adeleke, *Estimation of Solar Radiation over Ibadan from Routine Meteorological Parameters*, *The International Journal Of Engineering And Science (IJES)*, 4, 3 (2015) 44 – 51.
- [12] S. G. Abdu, A. S. Abdullateef, *Empirical Model for the Estimation of Monthly Global Solar Radiation in Zaria, Nigeria*. *International Journal of Physics and Mathematical Sciences*, 6, 4 (2016) 57 – 62.
- [13] G. M. Argungu, K. Dabai, *Application of Linear Models for Estimation of Global Solar Radiation using Available Meteorological Parameters for Sokoto, Nigeria*. *International Journal of Advances in Scientific Research and Engineering (ijasre)*, 3, 11 (2017) 76 – 83.
- [14] D. N. Girma, *Estimation of Monthly Average Daily Solar Radiation from Meteorological Parameters: Sunshine Hours and Measured Temperature in Tepi, Ethiopia*. *International Journal of Energy and Environmental Science*. Vol. 3, No. 1 (2018) 19- 26. <https://doi.org/10.11648/j.ijees.20180301.12>.
- [15] WMO, *A Note on Climatological Normal*. Technical Note. World Meteorological Organization, Geneva, Switzerland. (1967).
- [16] O. S. Ojo, B. Adeyemi, *Estimation of Solar Radiation using Air Temperature and Geographical Coordinate over Nigeria*, *The Pacific Journal of Science and Technology*, 15, 2 (2014) 78 – 88.
- [17] M. Iqbal, *An introduction to solar radiation*, first ed. Academic Press, New York. (1983)
- [18] S. Zekai, *Solar energy fundamentals and modeling techniques: atmosphere, Environment, climate change and renewable energy*, first ed. Springer, London. (2008)
- [19] E. O. Falayi, A. B. Rabi, R. O. Teliat, *Correlations to estimate monthly mean of daily diffuse solar radiation in some selected cities in Nigeria*, *Pelagia Research Library*, 2, 4 (2011) 480-490.
- [20] J.A. Prescott, *Transactions of the Royal Society of Australia* 48 (1940) 114-8.
- [21] H. Ogelman, A. Ecevit, E. Tasdemiroglu, *A new method for estimating solar radiation from bright sunshine data*, *Solar Energy*, 33 (1984) 619 – 25. [https://doi.org/10.1016/0038-092X\(84\)90018-5](https://doi.org/10.1016/0038-092X(84)90018-5).
- [22] T. D. M. A. Samuel, *Estimation of global radiation for Sri Lanka*, *Solar Energy*, 47 (1991) 333-337. [https://doi.org/10.1016/0038-092X\(91\)90026-S](https://doi.org/10.1016/0038-092X(91)90026-S).
- [23] F. J. Newland, *A study of solar radiation models for the coastal regions of South China*, *Solar Energy*, 31 (1988) 227 – 235. [https://doi.org/10.1016/0038-092X\(89\)90022-4](https://doi.org/10.1016/0038-092X(89)90022-4).

-
- [24] D. B. Ampratwum, A. S. S Dorvlo, *Estimation of solar radiation from the number sunshine hours*, *Applied Energy*, 63 (1999) 161 – 167. [https://doi.org/10.1016/S0306-2619\(99\)00025-2](https://doi.org/10.1016/S0306-2619(99)00025-2).
- [25] K. Bakirci, *Correlations for estimation of daily global solar radiation with hours of bright sunshine in Turkey*, *Energy*, 34 (2009) 485 – 501. <https://doi.org/10.1016/j.energy.2009.02.005>.
- [26] J. Almorox, C. Hontoria, *Global solar radiation estimation using sunshine duration in Spain*, *Energy Conversion and Management*, 45 (2004) 1529 – 1535. <https://doi.org/10.1016/j.enconman.2003.08.022>.
- [27] A. Louche, G. Notton, P. Poggi, G. Simonnot, *Correlations for direct and Global horizontal irradiation on a French Mediterranean site*, *Solar Energy*, 46 (1991) 261 – 266. [https://doi.org/10.1016/0038-092X\(91\)90072-5](https://doi.org/10.1016/0038-092X(91)90072-5).
- [28] R. Chen, K. Ersi, J. Yang, S. Lu, W. Zhao, *Validation of five global radiation Models with measured daily data in China*. *Energy Conversion and Management*, 45 (2004) 1759-1769. <https://doi.org/10.1016/j.enconman.2003.09.019>.
- [29] G. Hargreaves, Z. Samani, *Estimating potential evapotranspiration*. *Journal of Irrigation and Drainage Engineering*. ASCE, 108 (1982) 225-230.
- [30] J. V. Garcia, *Principios Físicos de la Climatología*. Ediciones UNALM (Universidad Nacional Agraria La Molina: Lima, Peru) (1994)
- [31] A. El-Sebaei, A. Trabea, *Estimation of Global Solar Radiation on Horizontal Surfaces Over Egypt*, *Egypt. J. Solids*, 28, 1 (2005) 163-175.
- [32] P. R. Bevington, *Data reduction and error analysis for the physical sciences*, first ed. McGraw Hill Book Co., New York (1969)
- [33] H. O. Merges, C. Ertekin, M. H. Sonmete, *Evaluation of global solar radiation Models for Konya, Turkey*. *Energy Conversion and Management*, 47 (2006) 3149-3173. <https://doi.org/10.1016/j.enconman.2006.02.015>.
- [34] M. B. Abdullahi, S. B. Sharafa, *Multivariable Empirical Equation for Estimation of Global Solar Radiation in Sokoto Nigeria*. *ATBU, Journal of Science, Technology & Education (JOSTE)*; Vol. 5, 3 (2017) 187 – 192.
- [35] O. O. Ajayi, O. D. Ohijeagbon, C. E Nwadialo, O. Olasope, *New Model to Estimate Daily Global Solar Radiation over Nigeria*. *Sustainable Energy Technologies and Assessments*, 5 (2014) 28 – 36. <https://doi.org/10.1016/j.seta.2013.11.001>.
- [36] L. Huashan, C. Fei, W. Xianlong, M. Weibin, *A Temperature-Based Model for Estimating Monthly Average Daily Global Solar Radiation in China*. *Hindawi Publishing Corporation. The Scientific World Journal*, Volume 2014 (2014) 1 – 9. <https://doi.org/10.1155/2014/128754>.

Instructions for Authors

Essentials for Publishing in this Journal

- 1 Submitted articles should not have been previously published or be currently under consideration for publication elsewhere.
- 2 Conference papers may only be submitted if the paper has been completely re-written (taken to mean more than 50%) and the author has cleared any necessary permission with the copyright owner if it has been previously copyrighted.
- 3 All our articles are refereed through a double-blind process.
- 4 All authors must declare they have read and agreed to the content of the submitted article and must sign a declaration correspond to the originality of the article.

Submission Process

All articles for this journal must be submitted using our online submissions system. <http://enrichedpub.com/> . Please use the Submit Your Article link in the Author Service area.

Manuscript Guidelines

The instructions to authors about the article preparation for publication in the Manuscripts are submitted online, through the e-Ur (Electronic editing) system, developed by **Enriched Publications Pvt. Ltd.** The article should contain the abstract with keywords, introduction, body, conclusion, references and the summary in English language (without heading and subheading enumeration). The article length should not exceed 16 pages of A4 paper format.

Title

The title should be informative. It is in both Journal's and author's best interest to use terms suitable. For indexing and word search. If there are no such terms in the title, the author is strongly advised to add a subtitle. The title should be given in English as well. The titles precede the abstract and the summary in an appropriate language.

Letterhead Title

The letterhead title is given at a top of each page for easier identification of article copies in an Electronic form in particular. It contains the author's surname and first name initial .article title, journal title and collation (year, volume, and issue, first and last page). The journal and article titles can be given in a shortened form.

Author's Name

Full name(s) of author(s) should be used. It is advisable to give the middle initial. Names are given in their original form.

Contact Details

The postal address or the e-mail address of the author (usually of the first one if there are more Authors) is given in the footnote at the bottom of the first page.

Type of Articles

Classification of articles is a duty of the editorial staff and is of special importance. Referees and the members of the editorial staff, or section editors, can propose a category, but the editor-in-chief has the sole responsibility for their classification. Journal articles are classified as follows:

Scientific articles:

1. Original scientific paper (giving the previously unpublished results of the author's own research based on management methods).
2. Survey paper (giving an original, detailed and critical view of a research problem or an area to which the author has made a contribution visible through his self-citation);
3. Short or preliminary communication (original management paper of full format but of a smaller extent or of a preliminary character);
4. Scientific critique or forum (discussion on a particular scientific topic, based exclusively on management argumentation) and commentaries. Exceptionally, in particular areas, a scientific paper in the Journal can be in a form of a monograph or a critical edition of scientific data (historical, archival, lexicographic, bibliographic, data survey, etc.) which were unknown or hardly accessible for scientific research.

Professional articles:

1. Professional paper (contribution offering experience useful for improvement of professional practice but not necessarily based on scientific methods);
2. Informative contribution (editorial, commentary, etc.);
3. Review (of a book, software, case study, scientific event, etc.)

Language

The article should be in English. The grammar and style of the article should be of good quality. The systematized text should be without abbreviations (except standard ones). All measurements must be in SI units. The sequence of formulae is denoted in Arabic numerals in parentheses on the right-hand side.

Abstract and Summary

An abstract is a concise informative presentation of the article content for fast and accurate Evaluation of its relevance. It is both in the Editorial Office's and the author's best interest for an abstract to contain terms often used for indexing and article search. The abstract describes the purpose of the study and the methods, outlines the findings and state the conclusions. A 100- to 250-Word abstract should be placed between the title and the keywords with the body text to follow. Besides an abstract are advised to have a summary in English, at the end of the article, after the Reference list. The summary should be structured and long up to 1/10 of the article length (it is more extensive than the abstract).

Keywords

Keywords are terms or phrases showing adequately the article content for indexing and search purposes. They should be allocated heaving in mind widely accepted international sources (index, dictionary or thesaurus), such as the Web of Science keyword list for science in general. The higher their usage frequency is the better. Up to 10 keywords immediately follow the abstract and the summary, in respective languages.

Acknowledgements

The name and the number of the project or programmed within which the article was realized is given in a separate note at the bottom of the first page together with the name of the institution which financially supported the project or programmed.

Tables and Illustrations

All the captions should be in the original language as well as in English, together with the texts in illustrations if possible. Tables are typed in the same style as the text and are denoted by numerals at the top. Photographs and drawings, placed appropriately in the text, should be clear, precise and suitable for reproduction. Drawings should be created in Word or Corel.

Citation in the Text

Citation in the text must be uniform. When citing references in the text, use the reference number set in square brackets from the Reference list at the end of the article.

Footnotes

Footnotes are given at the bottom of the page with the text they refer to. They can contain less relevant details, additional explanations or used sources (e.g. scientific material, manuals). They cannot replace the cited literature.

The article should be accompanied with a cover letter with the information about the author(s): surname, middle initial, first name, and citizen personal number, rank, title, e-mail address, and affiliation address, home address including municipality, phone number in the office and at home (or a mobile phone number). The cover letter should state the type of the article and tell which illustrations are original and which are not.

Address of the Editorial Office:

Enriched Publications Pvt. Ltd.
S-9, IInd FLOOR, MLU POCKET,
MANISH ABHINAV PLAZA-II, ABOVE FEDERAL BANK,
PLOT NO-5, SECTOR -5, DWARKA, NEW DELHI, INDIA-110075,
PHONE: - + (91)-(11)-45525005